Project Report
ATC-331

Technical Assessment of the Impact of Decommissioning the TDWR on Terminal Weather Services

J.Y.N. Cho
B.D. Martin

23 May 2007

Lincoln Laboratory
MASSACHUSETTS INSTITUTE OF TECHNOLOGY
LEXINGTON, MASSACHUSETTS

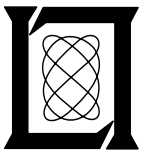

Prepared for the Federal Aviation Administration,
Washington, D.C. 20591

TECHNICAL REPORT STANDARD TITLE PAGE

1. Report No.	2. Government Accession No.	3. Recipient's Catalog No.
ATC-331		

4. Title and Subtitle	5. Report Date
Technical Assessment of the Impact of Decommissioning the TDWR on Terminal Weather Services	23 May 2007
	6. Performing Organization Code

7. Author(s)	8. Performing Organization Report No.
John Y.N. Cho and Brian D. Martin	ATC-331

9. Performing Organization Name and Address	10. Work Unit No. (TRAIS)
MIT Lincoln Laboratory 244 Wood Street Lexington, MA 02420-9108	11. Contract or Grant No. FA8721-05-C-0002

12. Sponsoring Agency Name and Address	13. Type of Report and Period Covered
Department of Transportation Federal Aviation Administration 800 Independence Ave., S.W. Washington, DC 20591	Project Report
	14. Sponsoring Agency Code

15. Supplementary Notes

This report is based on studies performed at Lincoln Laboratory, a center for research operated by Massachusetts Institute of Technology, under Air Force Contract FA8721-05-C-0002.

16. Abstract

Details of a technical study that was part of a larger investigation assessing terminal weather services impacts of decommissioning the Terminal Doppler Weather Radar (TDWR) are presented. Effects on two key areas for safety and delay-reduction benefits are examined: Low-altitude wind shear visibility and the Integrated Terminal Weather System (ITWS) Terminals Winds (TWINS) product. It is concluded that the information content provided by the TDWR cannot, in general, be effectively replaced by other candidate radar systems such as the Airport Surveillance Radar (ASR-9) equipped with a Weather Systems Processor (WSP) or the Next Generation Weather Radar (NEXRAD).

17. Key Words	18. Distribution Statement
TDWR, ITWS Terminal Winds, wind shear, WSP	This document is available to the public through the National Technical Information Service, Springfield, VA 22161.

19. Security Classif. (of this report)	20. Security Classif. (of this page)	21. No. of Pages	22. Price
Unclassified	Unclassified	68	

FORM DOT F 1700.7 (8-72) Reproduction of completed page authorized

EXECUTIVE SUMMARY

The Terminal Doppler Weather Radar (TDWR) is a high-performance radar designed (and operated) specifically for airport terminal area weather surveillance. The weather systems processor (WSP) is an add-on system for pre-existing airport surveillance radars (ASR-9s) that is also used for terminal-area weather sensing. Developed primarily to detect hazardous low-altitude weather phenomena, these systems have succeeded in eliminating wind-shear-related aircraft accidents at the sites where they have been deployed.

As they grow older, however, the costs of sustaining these systems increase, and this raises a concern. Even though the TDWR is a much more sensitive weather detector than the ASR-9 WSP, it is more expensive to maintain. Thus, the question has been asked whether the TDWR could be eliminated and WSPs installed instead at those airports without undue impact to terminal weather services.

In this report we present the results of a technical investigation into this question. Specifically, we examine the impact on safety (effects on the ability to sense low-altitude wind shear) and on delay reduction benefits (effects on the Integrated Terminal Weather System (ITWS) Terminal Winds (TWINDS) product). We consider the problem from both theoretical and empirical angles.

We conclude that decommissioning the TDWR will have a significantly negative impact on terminal-area safety. Even with the addition of the WSP to ASR-9s closest to the original TDWR sites, two airports would lose all wind-shear radar coverage, while 13 airports (including 7 of the top-20 busiest in the U.S.) would be left without acceptable microburst alert capability. Even if Next Generation Weather Radar (NEXRAD) data were to be used for gust-front detection and tracking, 61% of airports would lose adequate coverage in the 10-60 km range.

We also show that the ITWS TWINDS errors will increase dramatically at low altitudes in the terminal area, which will degrade the substantial delay reduction benefits currently reaped through the use of that product. Multi-Doppler coverage is the key to accurate wind vector estimates. The NEXRADs on their own are spaced too far apart to provide dual-Doppler coverage at low altitude over any TDWR airport. The degradation in wind estimate quality will be worst at some of the busiest terminal clusters such as New York, Chicago, Dallas, Houston, Miami, and Washington, D.C., where there are two or more TDWRs contributing to the TWINDS domain.

TABLE OF CONTENTS

LIST OF ILLUSTRATIONS

LIST OF ILLUSTRATIONS
(Continued)

LIST OF TABLES

1. INTRODUCTION

Currently the Federal Aviation Administration (FAA) has three radar systems capable of detecting low-altitude wind shear around airports. These are the Terminal Doppler Weather Radar (TDWR), the Airport Surveillance Radar-9 (ASR-9) Weather Systems Processor (WSP), and the Next Generation Weather Radar (NEXRAD). The first two are wholly owned and operated by the FAA for terminal area surveillance, while the funding and control of the third are shared with the National Weather Service (NWS) and the Department of Defense (DoD) for national-scale weather surveillance.

The TDWR was developed in response to a series of low-altitude wind-shear related aircraft accidents in the 1970s and early 1980s (Evans and Turnbull 1989). It is a stand-alone high-performance radar that is located off the airport site for optimal viewing geometry, which, however, makes it relatively expensive to deploy and maintain. As a lower-cost alternative to terminal-area wind-shear sensing, the WSP was developed as a piggyback processing system for already-existing ASR-9s (Weber and Stone 1995). The TDWRs were deployed at 45 high-risk sites and the WSPs were installed at 34 other airports (Figure 1-1). The mission has been a great success—there have not been any wind-shear caused aircraft accidents at the sites where these systems have been deployed.

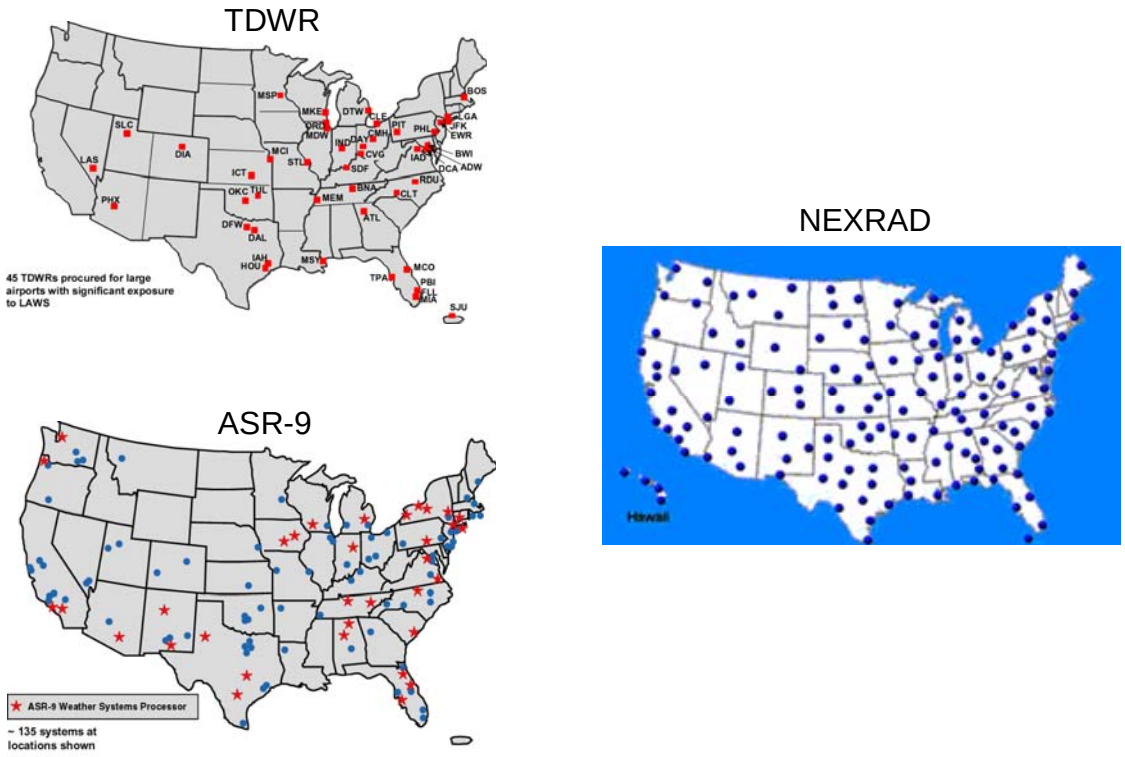

Figure 1-1. Locations of the TDWR, ASR-9, and NEXRAD systems. The ASR-9s with WSPs installed are shown as red stars.

The NEXRAD, like the TDWR, is a high-performance weather radar (Heiss et al. 1990). Its primary mission, however, is long-range weather surveillance, and as such, is not specifically sited near an airport. Its scan strategies are also not optimized for low-altitude wind-shear detection and the FAA does not have sole control of its operation.

As all three radar systems age, their maintenance costs rise. In fact, all three are either undergoing or will undergo substantial service life extension programs (SLEPs). Under this budgetary context, a suggestion was made to decommission all the TDWRs and replace their functionality by installing additional WSPs on ASR-9s and incorporating more NEXRAD data for terminal-area weather surveillance. The premise is that this move would cut costs substantially for the FAA. But what impact would this have on terminal weather services? This report examines this question from a technical perspective.

In evaluating the impact of decommissioning the TDWR on terminal weather services, we focused on two key areas for analysis: the low-altitude wind-shear detection and the Integrated Terminal Weather System (ITWS) Terminal Winds (TWINDS) products. The reason for focusing on the former is obvious. The primary driving force behind the creation of the TDWR was the desire to eliminate aircraft accidents due to hazardous low-altitude wind-shear phenomena. In considering the elimination of the TDWR, one must study carefully whether other existing radars can cover this critical safety issue with the same level of effectiveness.

However, as data generated by the TDWR have been incorporated more and more over the years into various terminal-area weather products, it has become clear that the benefit of having a highly sensitive, fine-resolution weather radar near an airport goes well beyond providing wind-shear alerts to controllers and pilots. One such product that relies heavily on TDWR data is ITWS TWINDS. A three-dimensional (3D) gridded wind-field product for the region around the airport, TWINDS optimally combines data from a numerical weather prediction model, Doppler weather radars, ground stations, and aircraft reports. Controllers use TWINDS information to plan around vertical wind-shear and high surface-wind events, as well as for forecasting wind shifts that require runway configuration changes. In the future, TWINDS may also be used to optimize the spacing of arrival flows, generate aircraft-path-based alerts of strong shear/turbulence segments, and provide improved wind-field analysis input for gust-front detection where current detector domains overlap. The annual estimated cost benefit of TWINDS for the New York City region (including direct operational costs and passenger time savings) is $62 million (Allan et al. 2001). For Atlanta, the figure is $3 million (Allan and Evans 2005). Benefits appropriately scaled from these two studies for some other high-delay airports are shown in Table 1-1. The total annual TWINDS cost benefit for just these airports is over $130 million.

TABLE 1-1

Estimated ITWS TWINDS Annual Benefit

Airport	Delay Savings (hrs)	Cost Savings ($M)
EWR JFK LGA	18,000	62
ORD	5,400	29
BOS	3,200	17
PHL	3,200	17
DFW	540	3
ATL	540	3

Although we did not conduct a technical study of it, low ceiling and winter weather observation is another area where TDWR data provide significant benefit to terminal weather services. Stratiform precipitation that accompanies low ceiling conditions and winter storms can be low-altitude phenomena that may be missed or underestimated by radars located relatively far from the airport (e.g., NEXRADs). ASR-9s are located at or near airports, but they provide little to no vertical resolution. Reference will be made to this issue when discussing the radar placement and viewing geometry in the following section.

In this technical analysis we produced statistics for each of the 45 TDWR airports plus LaGuardia (LGA), which is serviced using data from the JFK airport TDWR. Although NEXRADs are not considered to be terminal weather radars (i.e., they are not specifically sited near airports) and the FAA does not have full control or even top priority in their use, we included them in the wind-shear visibility study along with the ASR-9 WSP. The way the NEXRADs are currently used, their relatively slow (~5 minute) update rate is far from optimal for microburst detection. As the FAA is not the primary user of the NEXRAD, it may be difficult to implement a rapid-update mode specially designed for terminal area surveillance. In contrast, the TDWR conducts a surface scan in hazardous weather mode every ~50 s. NEXRADs can certainly be used for gust-front detection, however, as evidenced by the successful adaptation of the machine intelligent gust front algorithm (MIGFA) for NEXRAD data (Smalley et al. 2005). Thus, for a given airport, the combination of an ASR-9 WSP and a NEXRAD might be used to provide both microburst and gust-front detection capability in lieu of a TDWR.

2. IMPACT ON SAFETY: MICROBURST AND GUST-FRONT VISIBILITY

The ability of an algorithm to detect a wind-shear event from radar data is predicated on the radar visibility of the phenomenon. We define visibility as the probability of wind-shear signal to be strong enough to be distinguished from noise and clutter. Visibility is different from probability of detection (POD). To obtain detection the processing algorithm must be able to distinguish the wind-shear signature from all other signals that are also visible to the radar, while keeping the false-alarm rate at an acceptable level. Thus, wind-shear visibility is only the upper bound for wind-shear POD. The complex, fuzzy-logic nature of the detection algorithms makes them difficult to characterize analytically. Since the purpose of this study is to compare different radar systems rather than determine the absolute POD performance level of each one, we will only evaluate the low-altitude wind-shear visibility, specifically for microbursts and gust fronts. (There are other hazardous wind-shear occurrences, such as gravity waves and turbulence, but since the FAA does not have requirements for detecting these phenomena, we will not include them in this study.)

The radar visibility is principally determined by three factors: viewing geometry, signal-to-noise ratio (SNR), and signal-to-clutter ratio (SCR). Thus, in order to evaluate the theoretical wind-shear visibility of different radars, we need to know the 3D location of the radars and their sensitivity parameters, as well as the terrain information within their field of view. Let us first examine the viewing angle problem.

2.1 RADAR VIEWING GEOMETRY

The typical placement of weather and aircraft surveillance radars around a TDWR airport is depicted in Figure 2-1. For obvious reasons, the aircraft surveillance radar is usually located right at the airport. The location of the TDWR is determined by the balance of competing factors. The minimum observable height above ground decreases with distance to the airport. However, viewing geometries for microbursts and gust fronts are more favorable for radars located away from the airport. Also, large buildings such as hangars could block low-elevation-angle views from a radar located on the airport. It was determined that a distance of about 15 km from the center of the airport would be the best compromise for TDWR siting (Evans and Turnbull 1989). Specific azimuthal orientation depends on runway configuration and local terrain.

The NEXRAD, on the other hand, is not specifically a terminal surveillance system, so they can be any distance from airports.

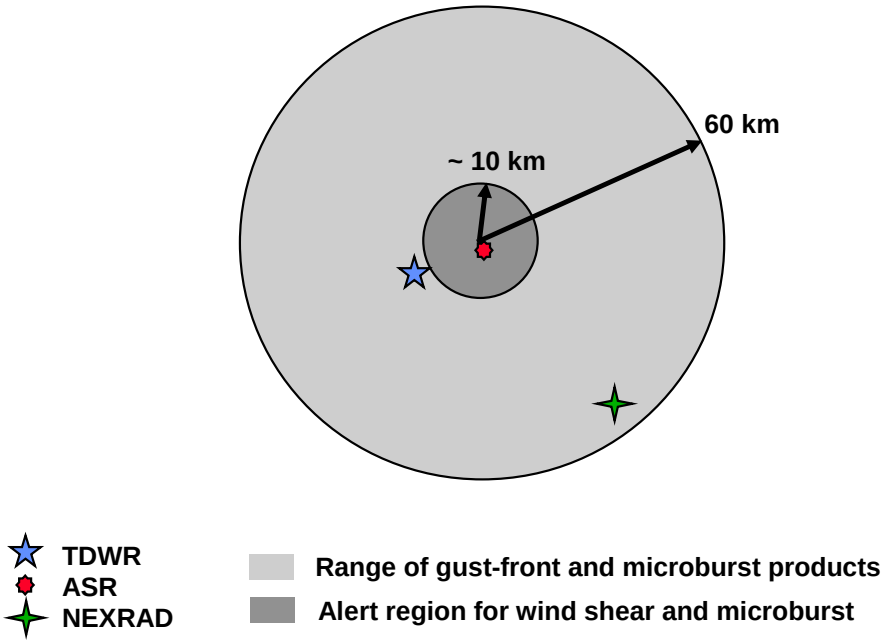

Figure 2-1. Typical weather and aircraft surveillance radar distances from a TDWR airport and the range of TDWR wind-shear products.

Although the TDWR produces base data out to a range of 90 km from the radar, its microburst and gust-front products only extend to 60 km from the airport, while wind-shear alerts are only generated within a small region around the airport (area noted for attention (ARENA) and microburst alert warning area (MAWA)) that is no more than about 10 km in radius (Figure 2-1). These range values roughly correspond to the initial detection range requirements (6 nmi for hazardous wind shear, microburst, and turbulence; 40 nmi for wind shifts and tornadoes) set by the FAA for the TDWR (FAA 1987). While the alert region is most critical for real-time flight safety, the far-range products are very useful for planning that can lead to delay reduction. We will divide our analysis results into near-range (0-10 km) and far-range (10-60 km) categories.

Wind-shear phenomena hazardous to aircraft that are landing at and taking off from an airport are at low altitude, especially microburst outflows. Therefore, there must be a requirement for minimum observable height above the airport for near-range (alert region) coverage. The further the radar is from the airport, the less it will be able to see near the ground due to the Earth's curvature. TDWRs can see at least down to 400 ft AGL at all associated airports (Figure 2-2). The average value is about 200 ft, which corresponds to an early FAA requirement (Interagency 1981). The calculation uses the location of the TDWR antenna (including height) vs. the airport coordinates, and uses the standard 4/3-Earth-radius approximation to account for atmospheric refraction. The radar beam is assumed not to scan below 0° elevation (true for all three radars at present). For our study, we will use 400 ft as the minimum required observable height.

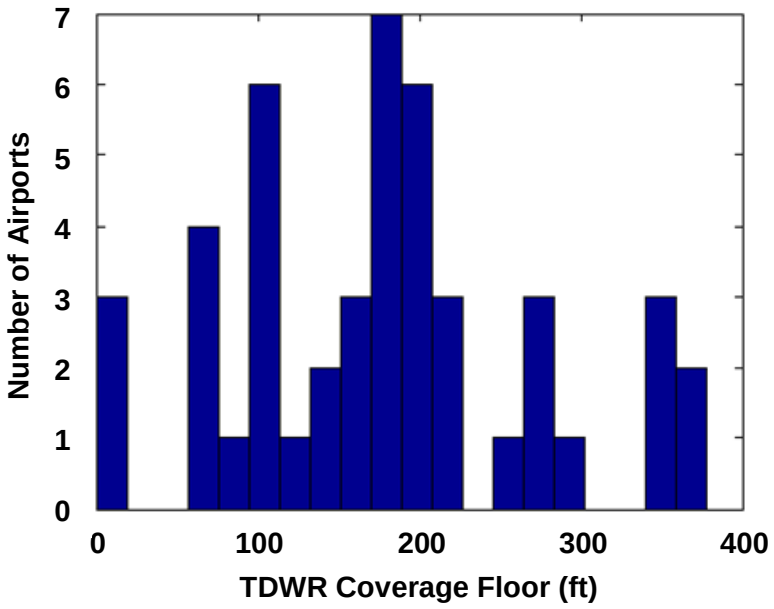

Figure 2-2. Histogram of minimum observable height above the airport ground level for all TDWRs.

To each TDWR airport we assign the nearest ASR-9 and NEXRAD. The resulting minimum observable heights above the airport ground level are shown in Figure 2-3. The red and blue lines indicate the 400-ft requirement for ASR-9 and NEXRAD. Of the 46 airports considered, two (West Palm Beach and San Juan) have neither an ASR-9 nor a NEXRAD close enough to provide the necessary low-altitude coverage. Of the remaining airports, 26 have alert-region coverage by an ASR-9 only and 18 have coverage by both ASR-9 and NEXRAD. The individual airports and the corresponding minimum observable height and distance to airport are listed in Table A-1 of Appendix A.

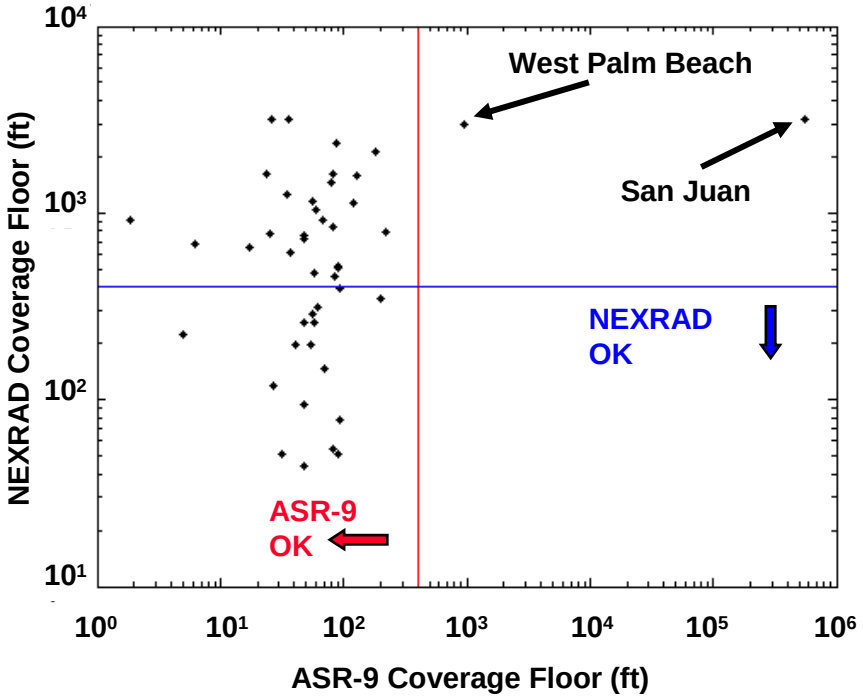

Figure 2-3. Minimum observable height above the airport ground level for the closest ASR-9 and NEXRAD to each TDWR airport.

The above calculation did not include terrain effects. Depending on the location, however, line-of-sight blockage can have significant impact on radar visibility. Thus, we computed the percentage of area around the airport blocked by terrain at a low elevation angle (0.3°, a typical value used by TDWRs for the surface scan) from the radar. Matlab functions from the Mapping Toolbox were used on Level 1 Digital Terrain Elevation Data (DTED) at 100-m horizontal resolution. The results were computed for a 10-km-radius circle and a ring of range 10-60 km around the airport. Of the 46 airports, only 16 had any blockage for any radar; the results are shown in Table 2-1. The NEXRADs tend to have the least amount of blockage, because they were sited for long-range (up to 460 km) surveillance. Although the elevation fan beam of the ASR-9 gives it visibility above the displayed 0.3° terrain blockage, it is still somewhat surprising that there is as much blockage as computed near the surface. Some of the ASR-9 antenna heights might be suspect, even though the best available information from the FAA was used. For example, the above-ground antenna height at DCA was listed at 16 ft, whereas direct visual observation (from an aircraft taxiing out) suggests that it is higher. Lacking better data, we proceeded with what we had.

TABLE 2-1

Percentage of Area Blocked by Terrain at 0.3° Elevation Angle

Airport	Radius Around Airport					
	0 – 10 km			10 – 60 km		
	TDWR	ASR-9	NEXRAD	TDWR	ASR-9	NEXRAD
BNA	0	0	0	21	14	0
BOS	0	6	0	0	16	0
BWI	0	1	0	0	17	0
CLE	0	0	0	0	10	9
DCA	0	62	0	0	80	1
DEN	0	2	0	17	15	11
EWR	0	6	0	23	34	0
IAD	0	0	0	18	15	17
LAS	0	32	0	90	83	9
PHL	0	0	0	0	3	0
PHX	8	10	1	58	52	32
RDU	0	2	0	0	2	0
SDF	0	6	0	0	20	0
SJU*	0	—	0	37	—	0
SLC	14	9	0	71	69	21
TUL	0	0	0	0	15	0

* SJU does not have an ASR-9 nearby. Unlisted airports have no blockage for any radar.

2.2 VISIBILITY RESULTS

To estimate the probability of a microburst or gust front being visible to the radar, we integrated over the measured probability distribution function for these phenomena and the specified coverage area, using the range-dependent minimum detectable reflectivity as the lower limit for the first integral. This method was based on a report by Weber and Troxel (1994) that assessed the weather detection capability of the ASR-11. Because that study assumed the radar to be located at the center of the airport, we generalized the equations to allow off-airport siting of the radar. We also included the effects of terrain blockage when the integrals are numerically evaluated, which was not done in the ASR-11 study.

At times the clutter level becomes the main hindrance to visibility rather than the receiver noise. To account for these cases, a separate integral was computed using a compiled probability distribution of clutter reflectivity and basing the lower limit of the inner integral on the subclutter visibility. Finally, a

joint visibility value was calculated of the noise-limited and the clutter-limited cases. The technical details of the entire procedure are presented in Appendix B.

The radar system characteristics are listed in Table 2-2. The weather sensitivity is computed as $P\tau G^2\Delta\theta\Delta\phi/\lambda^2$, where P is the peak transmitter power, τ is the pulse length, G is the antenna gain, $\Delta\theta$ is the elevation beamwidth, $\Delta\phi$ is the azimuthal beamwidth, and λ is the wavelength. The ASR-9 is nearly 20 dB less sensitive than the TDWR, while the NEXRAD is only 4 dB less sensitive. However, this metric does not include other factors that make the ASR-9 WSP and NEXRAD (especially the former) even less sensitive to low-altitude wind-shear events than the TDWR. A wider elevation beam means that phenomena confined near the ground (like microbursts and gust fronts) will fill a smaller fraction the beam, which makes the classical weather sensitivity metric an overestimate. Also, a weaker clutter suppression capability leads to lower visibility in clutter-limited environments. And a smaller number of pulses per coherent processing interval (CPI) results in increased base data variance. All of these factors are taken into account in computing visibility (Appendix B).

TABLE 2-2

Radar System Parameters

Parameter	TDWR	ASR-9 WSP	NEXRAD
Peak Power (kW)	250	1120	750
Pulse Length (μs)	1.1	1	1.6
Antenna Gain (dB)	50	34	45.5
Beamwidth (Az x El)	0.55° x 0.55°	1.4° x 4.8°	0.925° x 0.925°
Wavelength (cm)	5.4	11	10.5
Max. Clutter Suppression (dB)	60*	48	50
Rotation Rate (°/s)	~ 20	75	~ 20
CPI Pulses	~ 80	26	~ 50
Weather Sensitivity (dB)	115	96	111

* After radar data acquisition (RDA) system upgrade (Cho et al. 2005).

The resulting wind-shear event visibilities are divided according to wet vs. dry sites and whether or not the closest NEXRAD provides a low enough viewing angle for airport alert region (near-range) coverage. The median values for each of these categories are tabulated in Tables 2-3 through 2-6. West Palm Beach and San Juan data were not included in these medians, since these airports have no alert region coverage by an ASR-9 or a NEXRAD. We have somewhat arbitrarily assigned a color coding scheme of green (> 90%), yellow (80-90%), and red (< 80%) to the alert-area results based on the FAA goal of 90% POD for wind-shear events within this region (FAA 1987). (In practice, this "requirement" has only been applied to microburst detection and not gust-front detection, but for the purposes of this report we will reference this figure as a target for both wind-shear categories in the alert region.) In fact, a visibility of well above 90% would be needed, since the visibility is only an upper bound for the POD.

TABLE 2-3

Visibility for Wet Sites Without NEXRAD Alert Region Coverage (23 Sites)

Shear Type	Radius Around Airport					
	0 - 10 km			10 – 60 km		
	TDWR	ASR-9	NEXRAD	TDWR	ASR-9	NEXRAD
Microburst	100	93	0	68	27	28
Gust Front	98	88	80	97	3	50

TABLE 2-4

Visibility for Wet Sites With NEXRAD Alert Region Coverage (17 Sites)

Shear Type	Radius Around Airport					
	0 - 10 km			10 – 60 km		
	TDWR	ASR-9	NEXRAD	TDWR	ASR-9	NEXRAD
Microburst	100	93	99	68	28	63
Gust Front	98	89	99	97	3	85

TABLE 2-5

Visibility for Dry Sites Without NEXRAD Alert Region Coverage (3 Sites)

Shear Type	Radius Around Airport					
	0 - 10 km			10 – 60 km		
	TDWR	ASR-9	NEXRAD	TDWR	ASR-9	NEXRAD
Microburst	91	38	0	19	0	0
Gust Front	91	81	0	28	0	0

TABLE 2-6

Visibility for Dry Sites With NEXRAD Alert Region Coverage (1 Site)

Shear Type	Radius Around Airport					
	0 - 10 km			10 – 60 km		
	TDWR	ASR-9	NEXRAD	TDWR	ASR-9	NEXRAD
Microburst	95	41	93	31	0	40
Gust Front	99	87	95	80	3	82

First, as expected, the TDWR does very well in both microburst and gust-front visibility in the alert region. These are the categories most vital for safety concerns. It also does extremely well for gust-front visibility at far ranges for wet sites. For dry sites at far range, the numbers are down significantly due to the extensive terrain blockage at those sites (Table 2-1). Gust-front tracking throughout all ranges is most useful for traffic management, i.e., for delay reduction. Microburst detection beyond the near-range alert area is not an FAA requirement, so those numbers are not as important.

Second, in the 10-60 km region, the ASR-9 WSP is essentially useless for microburst and gust-front detection. Its sensitivity is simply not good enough to sense low-altitude wind-shear events at those ranges. Therefore, replacing TDWRs with ASR-9 WSPs without augmentation by NEXRAD data means the loss of wind-shear products at those far ranges.

Third, with visibility $\leq 41\%$, the WSP is also no good for detecting microbursts at dry sites even in the 0-10 km alert region. Dry-site performance of the WSP has always been a concern and the results

here quantitatively show why. Even for wet sites the gust-front visibility is ~89%, which makes it impossible to meet the 90% POD target.

NEXRAD, which is comparable in sensitivity to TDWR, has wind-shear visibility values that vary mainly with distance to the airport. If it is close enough, it has visibility that is similar to the TDWR, although at far ranges the additional beam-filling loss associated with its wider elevation beam degrades its performance relative to the TDWR. Even though its visibility in the alert region can be excellent, its current slow update rate is problematic for generating microburst warnings in a timely enough fashion.

Let us now look at the complete airport-by-airport listing of low-altitude wind-shear visibility (Table A-2 in Appendix A). For the TDWR, all near-range microburst visibilities are above 90%, except at SLC (85%). In fact, FAA studies have shown that the microburst POD at SLC is about 83%. This lower-than-desired figure has generated much discussion about how to improve it. Our analysis here shows that much of the problem lies in the extensive terrain blockage present at this site (Table 2-1).

We can use the 90% bound as a means of picking out airports that would be left with unsatisfactory microburst alert capability if the TDWRs were decommissioned; in other words, airports with no ASR-9 WSP providing 90% or greater alert-region microburst visibility. (We exclude NEXRADs for now because of their slow update rate.) These airports are: BOS, DAL, DCA, DEN, EWR, LAS, LGA, MDW, PBI, PHX, SDF, SJU, and SLC. Included in this list are 7 of the top-20 busiest airports in the United States in traffic movements (Airports Council International 2006): LAS (#5), DEN (#7), PHX (#8), SLC (#15), EWR (#16), BOS (#18), and LGA (#19). Note also that 2 out of 3 New York City area airports are on the list as well as the primary airport serving the nation's capital. Thus, even though these airports constitute a minority of the 46 airports served by TDWR, the overall negative impact on flight safety is expected to be quite significant.

One caveat to be noted here is that we used a uniform circular area to model the alert region, which is a simplification. Actual alert regions have irregular shapes with varying sizes. Therefore, it is possible that the terrain blockage factor may be significantly different for the alert region versus what we calculated for the 10-km circle around the airport (Table 2-1). Since TDWRs and ASR-9s are sited for good viewing of the alert region, their wind-shear visibility over the alert region may then be somewhat better than what we computed. This comment affects airports with significant terrain blockage in the 10-km circle in Table 2-1.

For gust-front detection and tracking at 10-60 km, the TDWR provides good visibility (> 80%) at 38 airports. Assuming that NEXRAD data could be used for this task, only 15 airports would retain the same or better level of visibility, which is a reduction of 61% in the number of airports with long-range gust-front products.

3. IMPACT OF DELAY REDUCTION BENEFITS: THE ITWS TWINDS PRODUCT

As explained earlier, the ITWS TWINDS product provides a substantial cost benefit in direct operational costs and passenger time savings through delay reduction. The TDWR data stream is fed as input to TWINDS and is crucial in providing low-altitude coverage and good vertical resolution in the airport region. Thus, we wished to find out what happens to the quality of the TWINDS output if the TDWR data stream is cut off. We approached this question from both theoretical and empirical perspectives. For this analysis we included the Teterboro, NJ airport (TEB), since it is serviced by ITWS that ingest data from the New York City area TDWRs.

3.1 THEORETICAL ANALYSIS

TWINDS is a 3D gridded wind-field product that assimilates data from the Rapid Update Cycle (RUC) numerical weather prediction model, TDWRs, NEXRADs, aircraft weather reports, and ground observation sensors in an optimal manner. The output has a temporal resolution of 5 minutes with a horizontal resolution as fine as 1 km layered at a vertical resolution of 25 mb from 1000 mb (360 ft MSL) to 100 mb (53,000 ft MSL) (Cole and Wilson 1994). The errors in the output winds are dependent on the errors of the input data combined with geometric factors and displacement errors. For this study we calculated the output vector wind errors for a 120 x 120-km domain around each TDWR airport for the two lowest pressure levels above the airport ground level. We excluded ground station and aircraft data, since they tend to be sparse (and sporadic in the latter case). This omission should not affect the results very much because we are interested in the change in output error rather than the absolute error values. Displacement errors were also ignored for radar data assimilation, but the error differences are not expected to be very sensitive to this, either. Technical details of the error computation are given in Appendix C.

First, we give an example of the computed difference in output wind error for the New York City terminal region. Figure 3-1 shows the results for the 360-ft level. Without the TDWR data input the vector wind error is mostly pegged to the RUC input error of ~7 m s^{-1}. One can see the influence of the closest NEXRADs barely coming into view from the southwest and east. However, without dual-Doppler overlap, the improvement is not great. With the TDWR data the errors are reduced to ~1 m s^{-1} in the near-terminal area. The overlap in coverage of the two TDWRs yields dual-Doppler information, which makes this dramatic improvement in vector wind error possible. Figure 3-2 shows similarly significant differences in wind error with and without the TDWR at the next highest level (1060 ft). One can see as the height increases that the radars' fields of view expand. So the value of TDWR data is highest at the lowest altitudes.

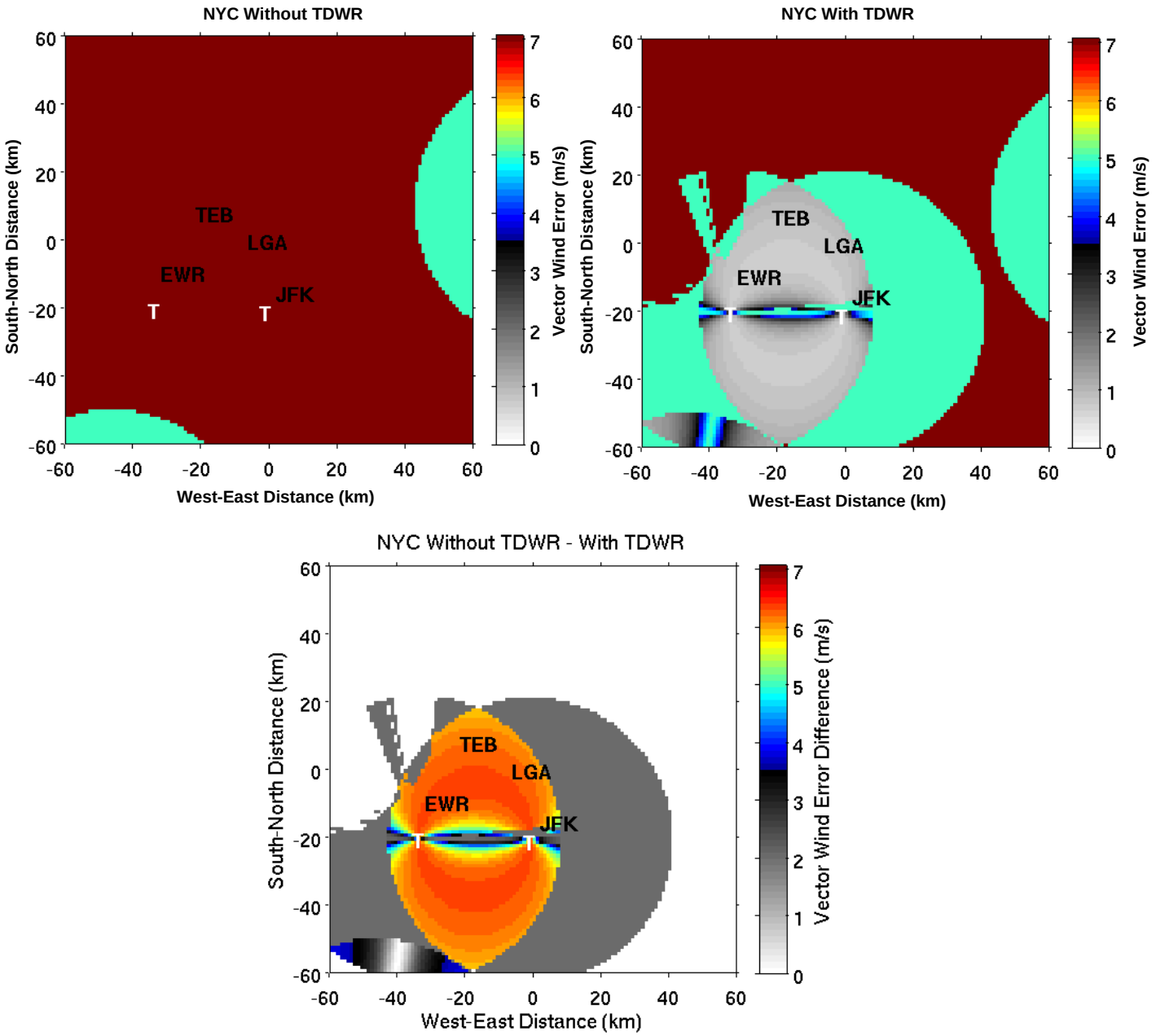

Figure 3-1. Vector wind error for the New York City region for the 1000-mb (360 ft MSL) level: (top left) without TDWR data, (top right) with TDWR data, and (bottom) difference between the two cases. TDWR locations are indicated by the "T"s.

Vector wind errors averaged over an area around each TDWR airport are summarized as distributions in Figure 3-3. Again the difference between having and not having TDWR data as input to TWINDS is clear and substantial.

Note that TWINDS does not currently ingest ASR-9 WSP data. This is due to the poor vertical resolution of the ASR-9 radar. There may be a limited contribution that WSP could make to TWINDS at very short range, but it cannot be expected to replace much of the coverage lost if TDWRs were to be eliminated.

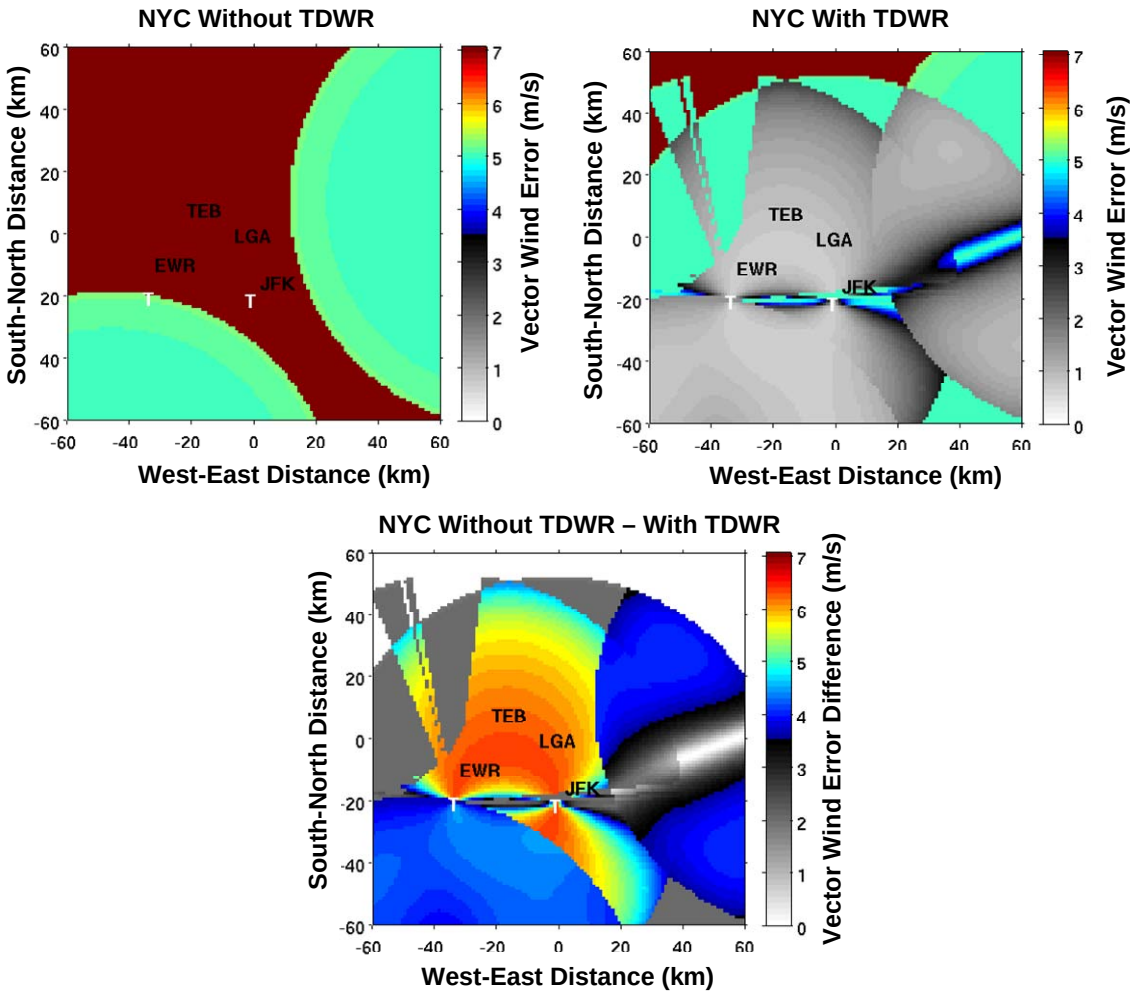

Figure 3-2. Same as Figure 3-1 except for the 975-mb (1060 ft MSL) level.

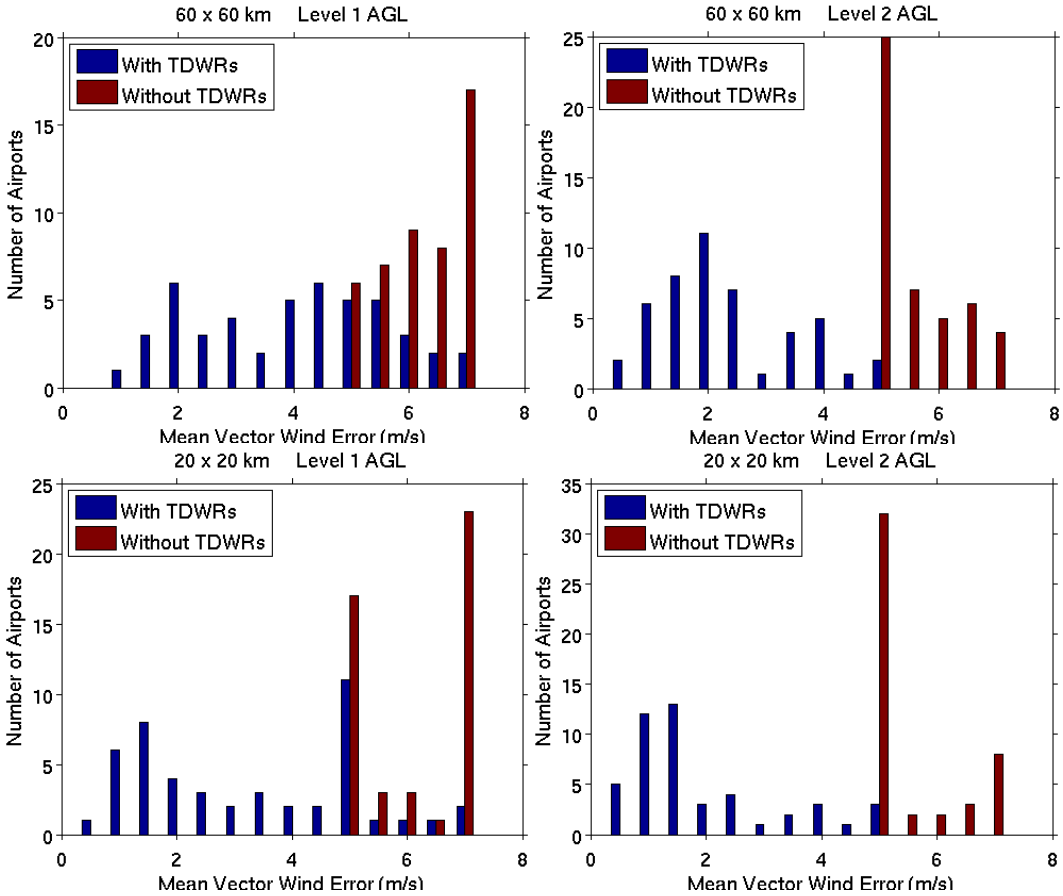

Figure 3-3. Vector wind errors averaged over a 60 x 60 km (top) and 20 x 20 km (bottom) domain around each TDWR airport for the lowest (left) and second lowest (right) pressure levels above the airport ground level.

The airport-by-airport results are listed in Table A-3 of Appendix A. The greatest loss in TWINDS accuracy is experienced at airports that are within ITWS domains that utilize data from multiple TDWRs (Table C-1): Chicago, Dallas, Houston, Miami, New York, and Washington, DC. These domains also include some of the highest delay-reduction benefit airports for TWINDS (Table 1-1).

At higher altitudes, the NEXRADs that are located far away from the airport terminal area will be able to contribute more information to the TWINDS domain. However, even if the data from the maximum Doppler range are assumed to be available, the impact of losing TDWR data is substantial. This is because the addition of TDWR data allows the near-terminal domain to have extensive multi-Doppler coverage, which dramatically improves vector wind estimates.

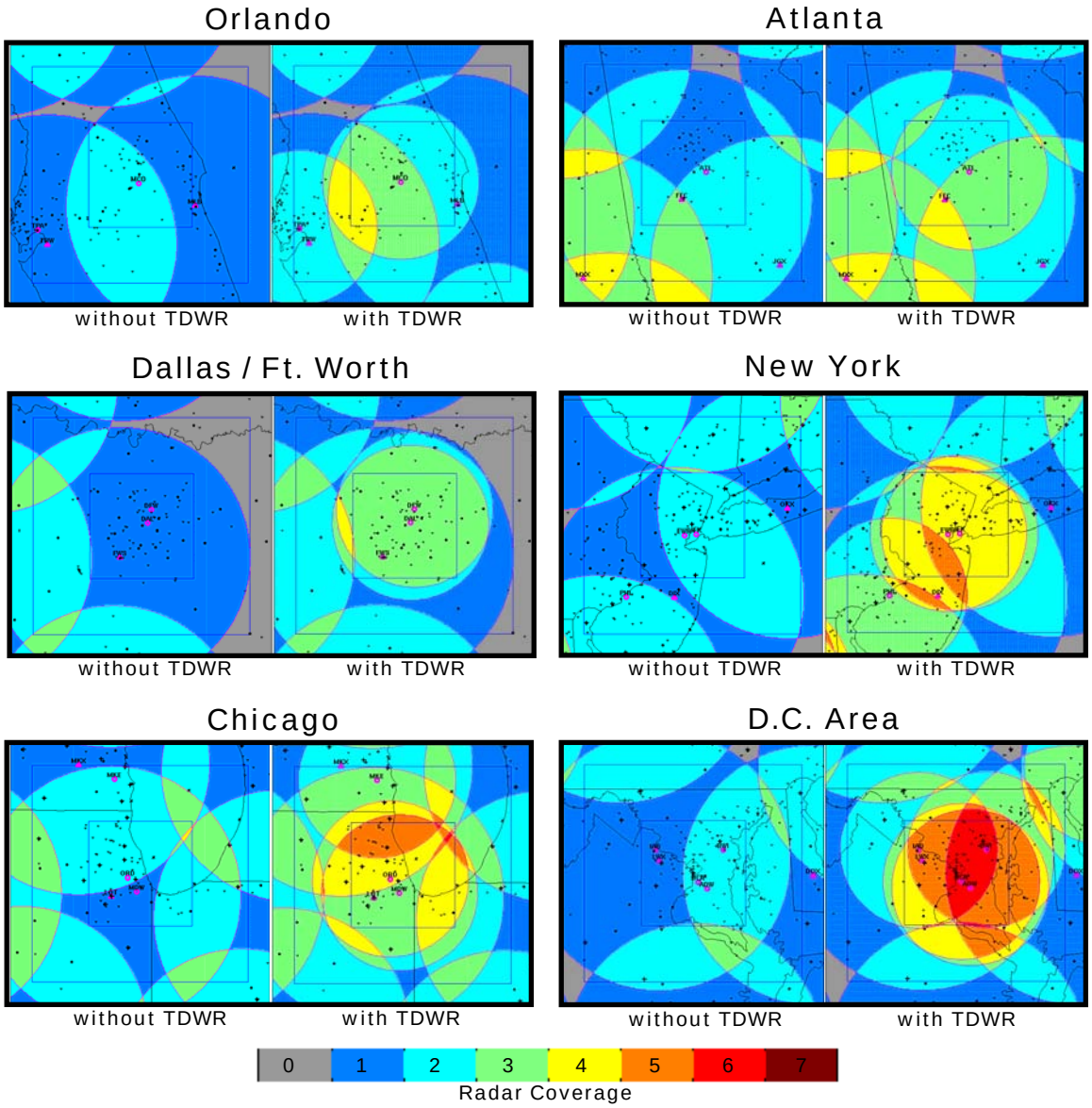

Figure 3-4. Radar coverage reduction that results from the exclusion of TDWRs. Maximum Doppler range is assumed. The color scale shows the number of radars providing coverage for a particular region. Left-side images of each comparison set show the reduction of coverage that result when only NEXRADs provide data input. Right-side images of the comparison sets include both NEXRADs and TDWRs.

Figure 3-4 is a simple illustration of the effect removing TDWRs would have on multi-Doppler TWINDS coverage at selected major airports. Images are color coded by the number of radars that provide coverage (for maximum Doppler range) in a given geographical area. Notice the large reduction in multi-Doppler coverage that would occur in the near-terminal area without the TDWR. The situation is, of course, much worse at low altitudes, where the visibility range of the radars become much shorter than their maximum range. At the major hubs of New York City, Washington, DC, and Chicago, much of the multi-Doppler wind retrieval would only be facilitated by distant NEXRADs, providing little improvement in wind estimates over the RUC input at critical low altitudes. This reduction is most prevalent in the DC area, where four TDWRs are positioned inside the fine-analysis domain. The bottom line is that NEXRADs are spaced too far apart to provide adequate multi-Doppler coverage in the terminal area at most TDWR airports.

3.2 EMPIRICAL ANALYSIS

We now examine three real-life wind-shear cases and compare the TWINDS output with and without TDWR input data. The examples consist of a convective event in the Dallas area and two wind-shear events over the New York City airports. Results show that eliminating TDWR data input to the algorithm significantly reduces the TWINDS ability to properly resolve wind-shear events, especially at critical near-terminal low altitudes. Poor resolution of these types of near-terminal wind events can lead to an increase in operational costs as well as pose the risk of reducing a controller's ability to conduct safe operations.

3.2.1 Dallas Convective Weather Event of 27 June 2000

Figure 3-5 shows the sensor configuration of the TWINDS domain over DFW. The coarse- (10 km) and fine-scale (1 km) analysis domains are outlined in blue. The array of ground sensors made available to TWINDS are depicted by symbols denoted in the map key. The primary radars consist of the single FWS NEXRAD in the southwest quadrant of the fine analysis grid, the DFW TDWR, and the DAL TDWR. Magenta circles outline the range of retrievable Doppler velocities from any particular radar. At low altitudes this range will be shorter due to the Earth's curvature. Secondary radar data from outside the TWINDS domain could be ingested and their range rings have also been outlined, but in the case of this domain no near-terminal benefit would be realized through their addition.

In the afternoon of 27 June 2000, a convective weather event broke out over the Dallas/Ft. Worth area. Aircraft delays were substantial with numerous ground stops and several missed approaches due to convection impacting the near-terminal area. Strong convective elements initially developed in the northwest quadrant of the TWINDS fine-scale grid. The convection produced a vigorous outflow boundary that traversed the entire diagonal length of the 121 x 121 km fine-analysis domain initiating new convection along its wake. Significant hydrometeors and dust allowed this event to be well captured by all three primary radars in both reflectivity and Doppler velocity returns. At 20:15Z, the outflow

boundary crossed the DFW airport and was sensed by the Low Level Wind Shear Alert System (LLWAS). Red vectors at the center of each image in Figure 3-6 depict the LLWAS measurements at 20:15Z. Note that LLWAS is a suite of surface measurements that do not change with the altitude of the TWINDS analyses (as denoted in Figure 3-6).

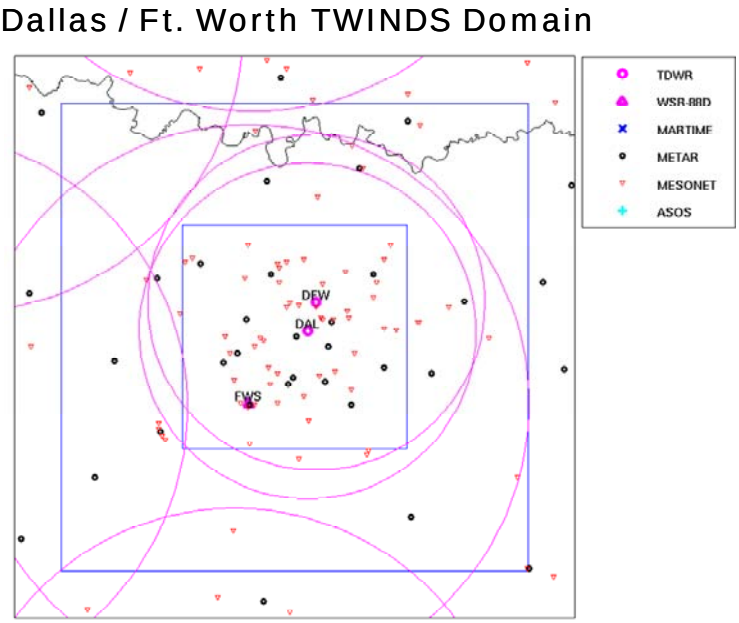

Figure 3-5. The sensor configuration for TWINDS over DFW consists of an array of ground sensors, the DFW and DAL TDWRs, and the single FWS NEXRAD. Magenta circles indicate the maximum range of retrievable Doppler velocity data from radars in the region.

Two separate TWINDS analyses of this event have been constructed for comparison. One analysis excludes the TDWR data as input to TWINDS and the other includes TDWR data in the input suite. A near-surface (1000 mb to 950 mb) side-by-side comparison of TWINDS analyses is shown in Figure 3-6. Yellow vectors in the left column of images show the resulting TWINDS analysis with TDWR inputs removed, yellow vectors in the right column of images show the resulting TWINDS analysis including TDWR. Composite reflectivity (dBZ color scale) from the DFW TDWR is used to illustrate the intensity of convection and the location of the outflow boundary as it crosses the airport at 20:15Z. The location of each radar center is labeled in red for reference.

Immediately noticeable in the side-by-side comparison is that the convective outflow due north of DFW is not resolved in the TWINDS analysis that excludes DFW and DAL TDWR inputs. This is evident in all vector fields down the left column of Figure 3-6. The divergent pattern of this convective element, typical of thunderstorm outflow, is clearly resolved when the TDWR data are included in the TWINDS input (vector fields down right column of Figure 3-6).

Absent from the no-TDWR analysis is the operationally significant outflow boundary that crosses the DFW airport at 20:15Z. At the 1000-mb and 975-mb layers of the analysis, the FWS NEXRAD data cannot provide the information necessary to resolve the boundary at low levels on its own. The boundary is only weakly realized at the 950 mb layer of the no-TDWR analysis. The 950-mb layer is at an altitude where more NEXRAD data are valid. Still, the analysis needs the TDWR inputs to better realize the boundary in the vector field (as is seen in the right side column of Figure 3-6).

To better quantify the differences in the two TWINDS analyses, the near-airport vector fields of both analyses were compared to a measure of truth—the LLWAS sensor suite wind measurements. Vector errors were constructed by comparing each LLWAS wind measurement to its nearest counterpart in both TWINDS vector fields. Figure 3-7 is a time series of the root-mean-square error (RMSE) of the two TWINDS analyses as compared to LLWAS at the near-surface layer of 1000 mb during the 27 June 2000 convective weather event. The red-dashed lines are the RMSE of the east-west wind component (u), the blue–dashed lines are the RMSE of the north-south wind component (v), and the solid black lines are the RMSE of the wind magnitude (V). Notice that at the time when the outflow boundary crosses the DFW airport (20:15Z, as indicated by the solid red vertical bars), the RMSE of v and V are doubled in the TWINDS analysis that does not utilize TDWR data (left plot of Figure 3-7).

3.2.2 New York City Wind-Shear Event of 20 December 1999

Figure 3-8 shows the sensor configuration within the TWINDS domain over NYC. Once again, the coarse- and fine-analysis domains are outlined in blue with the depiction of ground sensors noted in the map key. Primary radars for this domain are two NEXRADs and two TDWRs. The NEXRADs are DIX just south of the fine-analysis domain and OKX to the east of the fine-analysis domain. The TDWRs are the EWR and JFK radars, located near the center of the fine-analysis domain. As stated previously, secondary radars outside the TWINDS domain have also been outlined but have been excluded from the sensor suite because no near-terminal benefit would be realized through their addition. A third TDWR could include PHL, but its limited range into the fine-analysis domain warrants exclusion.

On 12 December 1999, a significant large-scale wind shear event occurred over the NYC region. Weak scattered precipitation accompanied an approaching cold front. As the warm sector of the system pushed through the NYC region, winds veered strongly with height, from easterly at 1000 mb to southerly at 800 mb (see Figure 3-9). A full 180° of directional shear occurred on this day between the surface and 400 mb.

The main cause of operational impact was this strong vertical wind shear. Widespread directional wind shear affected the northeast corridor and led to delays exceeding an hour at Newark International Airport and up to 4 hours at LaGuardia Airport. Increasing winds throughout the evening caused numerous missed approaches at the major NYC airports as the result of excessive tailwinds. Implementation of unplanned runway configuration changes to mitigate wind-shear impacts further compounded delay.

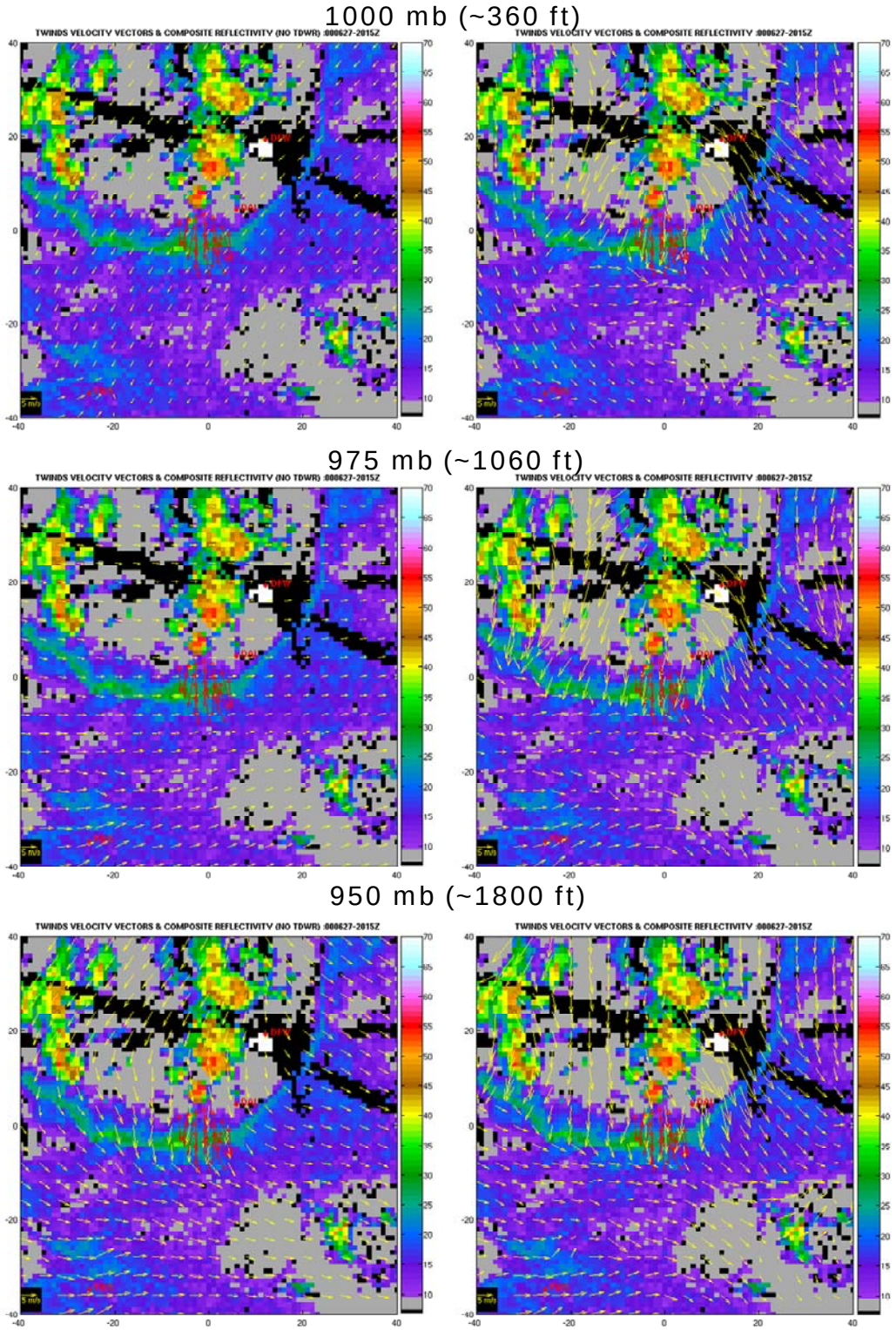

Figure 3-6. 1000 mb to 950 mb layer TWINDS comparisons during a convective weather event over Dallas–Fort Worth International Airport. Left column are the TWINDS analyses utilizing radar inputs from only the FWS NEXRAD, right column are TWINDS analyses utilizing radar inputs from both NEXRAD and TDWRs. Yellow wind vectors (m s^{-1}) lie atop radar composite reflectivity from the DFW TDWR (dBZ). Red vectors at the center of the grid are LLWAS wind measurements used to truth both TWINDS analyses.

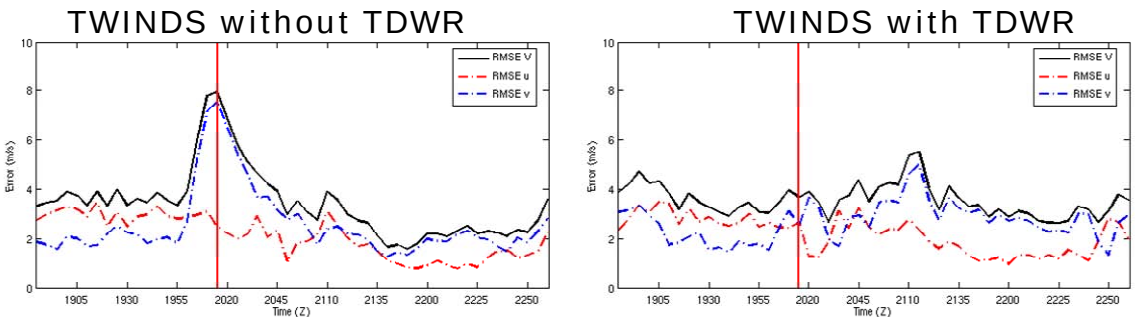

Figure 3-7. TWINDS RMS errors of 1000-mb wind analysis when truthed against LLWAS at Dallas-Fort Worth International Airport. The red dashed line is a time series of RMSE of the east-west component (u) of the wind analyses, the blue dashed line is a time series of RMSE of the north-south component (v) of the wind analyses, the solid black line is the RMSE of the wind magnitude (V).

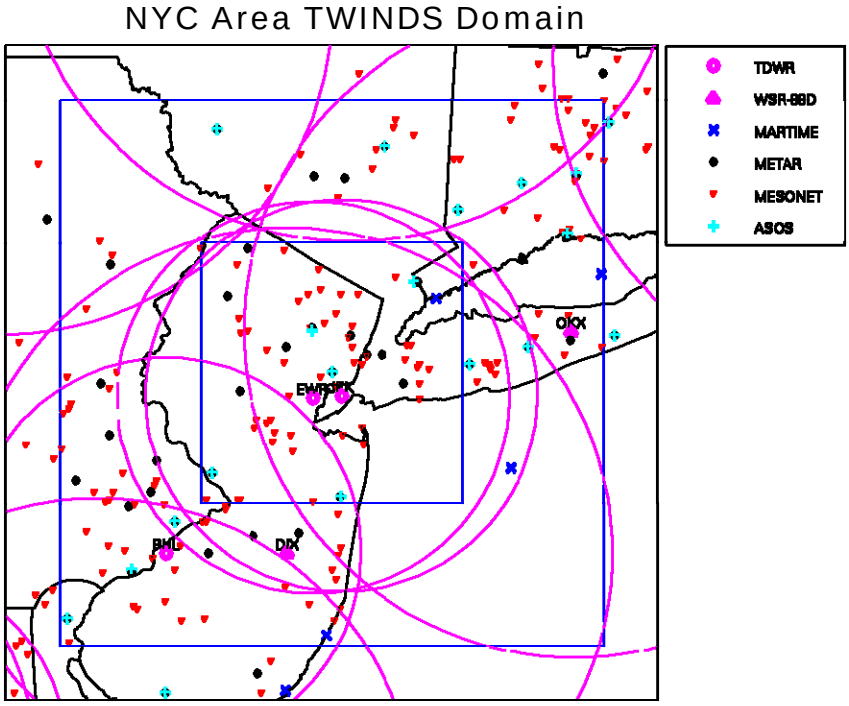

Figure 3-8. The sensor configuration for TWINDS over New York airports consists of an array of ground sensors, EWR and JFK TDWR, the DIX NEXRAD to the south, and the OKX NEXRAD to the east of the 1km domain. Magenta circles indicate the maximum range of retrievable Doppler velocity data from these and other radars in the vicinity.

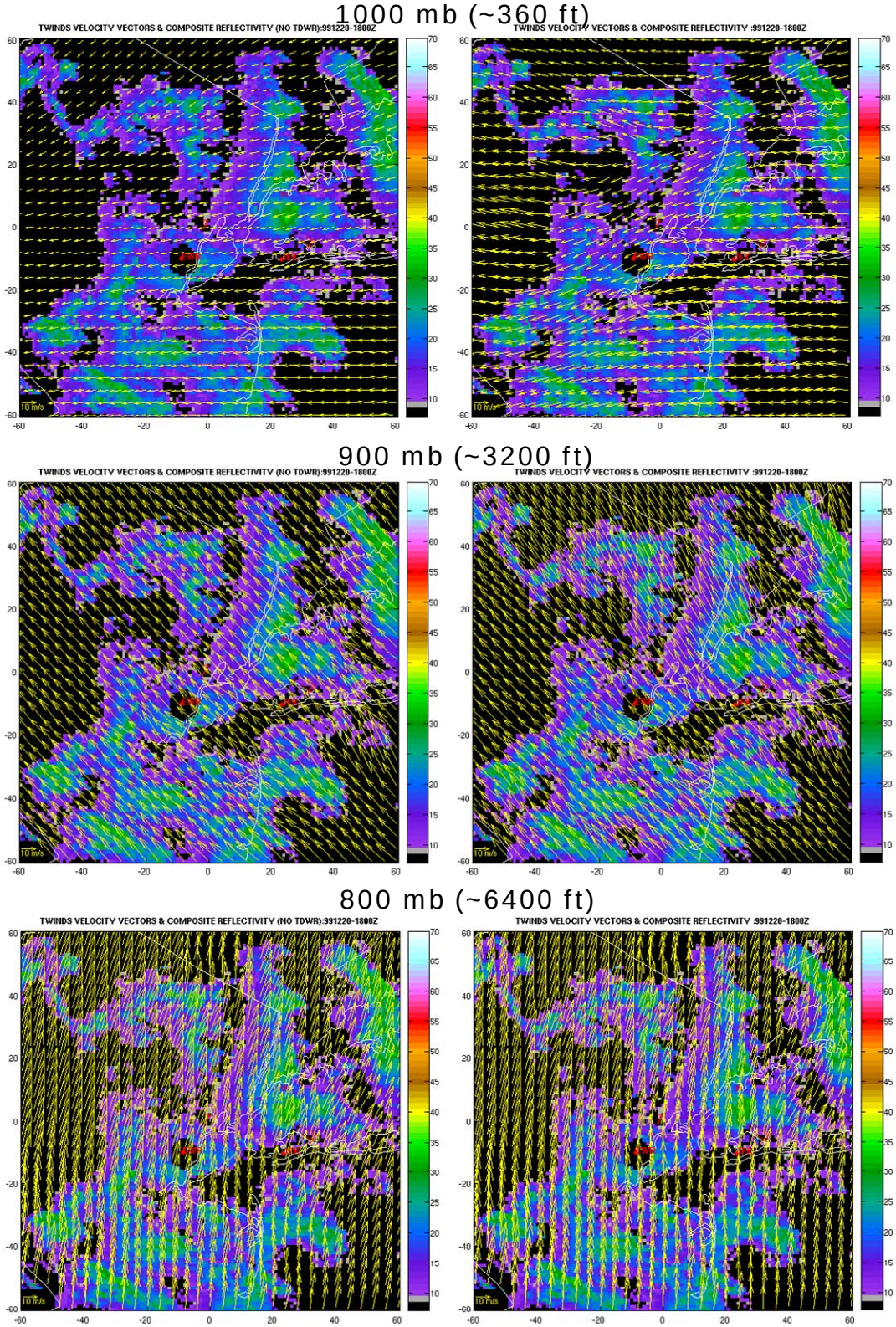

Figure 3-9. 1000-mb, 900-mb, and 800-mb layer TWINDS comparisons during a strong vertical wind-shear event. In the left column are the TWINDS analyses utilizing inputs from the DIX and OKX NEXRADs, in the right column are TWINDS analyses utilizing radar inputs from both NEXRADs and TDWRs. Yellow wind vectors (m s^{-1}) lie atop radar composite reflectivity from the EWR TDWR (dBZ). 90° of directional shear occurs between the 1000-mb and 800-mb analysis layers, 180° of directional shear occurs between the 1000-mb and 400-mb levels (layers above 800 mb not shown).

In Figure 3-9, side-by-side comparisons show that the largest differences between the two TWINDS analyses occur at low levels. This can be illustrated by visually comparing the two 1000-mb vector fields at a time that best represents the wind-shear event (the 18:00Z images in the first row of Figure 3-9). The left-side image shows that the analysis excluding JFK and EWR TDWR inputs produces a relatively uniform vector field with comparatively low wind magnitudes (with average winds of less than 10 m s^{-1}). Due to their distant locations the DIX and OKX NEXRADs cannot observe much down at the 1000-mb level in the middle of the domain, meaning that the left-side analysis at this layer is made up of inputs dominated by RUC (RUC produces a forecast every hour with a latency of roughly an hour). On the other hand, the right-side vector field at this layer is heavily influenced by rapid data updates from the centrally located TDWRs (full volume scans are completed within six minutes with very little latency).

Visually comparing the higher altitude layers, differences between the two TWINDS analyses become more subtle. The 900 mb side-by-side comparison shows that the vector fields differ mainly in wind magnitude with the TWINDS that includes TDWR as inputs analyzing slightly stronger winds. From 800 mb and above, slight differences in the two analyses become irrelevant.

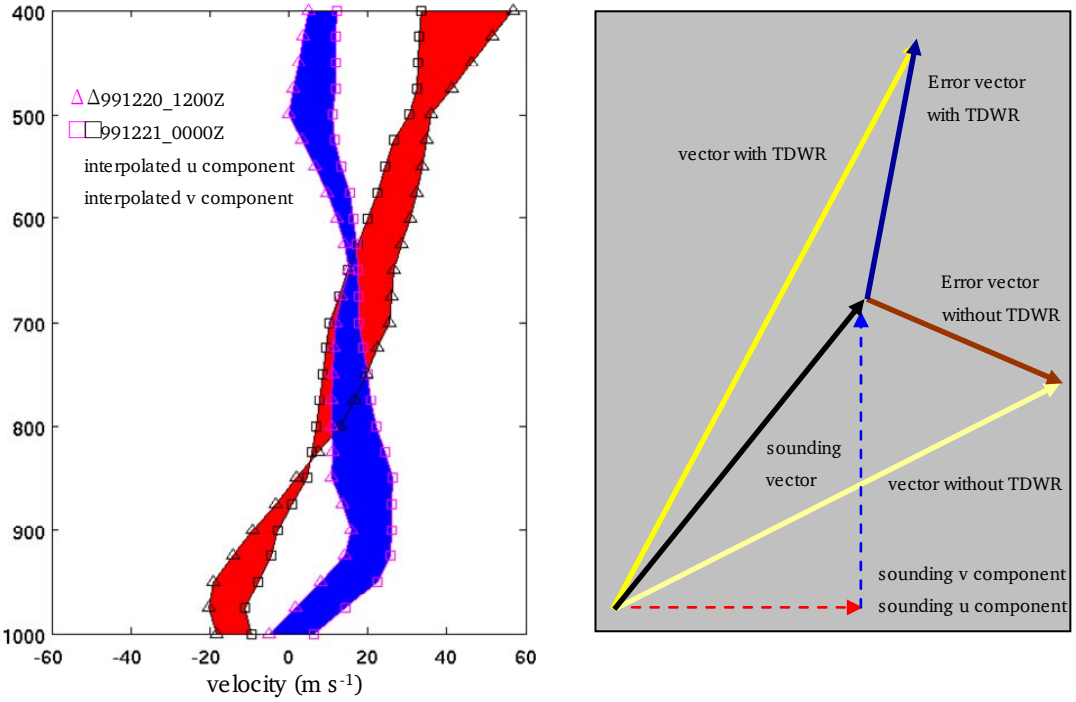

Figure 3-10. Left: Swath of time-interpolated soundings used as truth in TWINDS analysis comparison. Each vector in the fine-analysis grids has been differenced against the corresponding sounding point for that time and layer. Differences in wind components between TWINDS analyses make up the population of vector errors for the comparisons. Right: Diagram of the error vector computation.

The two TWINDS analyses of this wind shear event have been compared to radiosonde data from the OKX site, which are held as truth for the event. The full analysis time of the event spans 17:30Z to 20:00Z with vector fields produced at a five minute interval. Given that soundings are launched twice daily at 00:00Z and 12:00Z, a set of time-interpolated soundings that match the update rate of the TWINDS analyses were constructed from the soundings that bound the event. Because the synoptic front remained west of the analysis domain producing gradual changes in wind speed and direction, soundings were linearly interpolated through time. A visual representation of the constructed soundings is provided in the left side image of Figure 3-10: The red swath represents the time-interpolated east-west component of the soundings (u) and the blue swath represents the north-south component (v).

Each analysis vector has been differenced against its corresponding pressure and time sounding point. This provides roughly 440,000 error vector samples per layer for each of the TWINDS analyses. A diagram of the error vector computation is illustrated in the right-side image of Figure 3-10. Magnitudes of the blue and brown error vectors make up the quantitative comparison for this 20 December 1999 wind-shear event.

Figure 3-11 is a series of box plots and histograms of TWINDS comparison layers from 1000 mb up through 825 mb. Blue boxes and distributions represent the error vector magnitudes ($|V_{ERROR}|$) of the TWINDS analysis utilizing TDWR as input. Brown boxes and distributions represent $|V_{ERROR}|$ where TDWR data were not included in the input suite. Boxes bound the inner quartile range of the corresponding $|V_{ERROR}|$ distributions. Median $|V_{ERROR}|$ are denoted by the red bar height inside each box. Note that these are notched box plots, but due to the large size of the $|V_{ERROR}|$ population, uncertainty about the median is irrelevant as notches are indistinguishable from straight lines. This indicates that any visible difference in the median $|V_{ERROR}|$ between analysis layer comparisons is statistically significant.

In a layer-by-layer comparison of TWINDS $|V_{ERROR}|$, the greatest benefit through the utilization of TDWR data is achieved in the boundary layer of the atmosphere between the analysis layers of 1000 mb to 900 mb. Here, medians are well separated with all median $|V_{ERRORS}|$ for the analyses excluding TDWR being larger. In some instances (at the 1000-mb and 925-mb layers) median $|V_{ERRORS}|$ are almost doubled by excluding TDWR. While, for example, a 1000-mb median $|V_{ERROR}|$ difference of roughly 5 m s^{-1} seems insignificant, these $|V_{ERRORS}|$ operationally translate to a difference between ~10 kts including TDWR and ~20 kts excluding TDWR, differences which can translate into missed approaches or delayed/premature runway configuration changes.

Only in the single analysis layer of 825 mb does the median $|V_{ERROR}|$ of the analysis including TDWR exceed the median $|V_{ERROR}|$ of the no-TDWR analysis. Beyond 825 mb, while differences in $|V_{ERROR}|$ distributions of the two TWINDS analyses do exist and resemble the distributions seen at the 850-mb layer, the median $|V_{ERRORS}|$ become statistically indistinguishable.

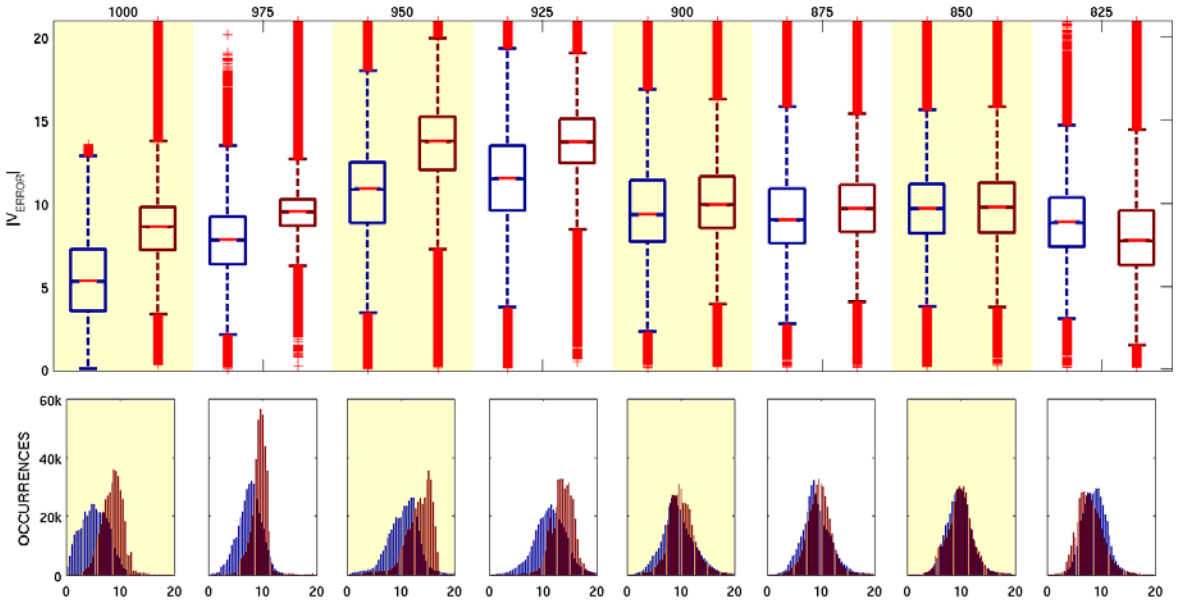

Figure 3-11. Series of box plots and histograms of TWINDS comparison layers from 1000 mb (left column) up through 825 mb (right column). Blue boxes and distributions represent the error vector magnitudes of TWINDS analyses utilizing TDWR as inputs. Brown boxes and distributions represent TWINDS analyses errors where TDWR were not included in the input suite. Units along the ordinate of the box plot diagram and the abscissas of the histograms are in m s^{-1}.

3.2.3 New York City Wind-Shear Event of 29 APRIL 2002: Uncontrolled Descent of a Boeing 767 on Final to JFK

On 29 April 2002, between 00:58Z and 00:59Z, a Boeing 767 on final approach from SFO to JFK experienced an uncontrolled descent of 1200 ft in less than 1 minute. A time vs. height plot is denoted by the blue line in the right-side image of Figure 3-12. Red vectors in the left-side image shows the instantaneous heading of the 767 with flight times denoted along the path. Losses encountered on final approach are associated with a strong shear boundary attributed to eastward propagating buoyancy waves interacting with spawned convection. The previous arrival experienced reductions in airspeed and suggested that Air Traffic Control at JFK vector subsequent arrivals tighter to the field so that weather approaching from the west could be avoided. None of the JFK surface alert systems in place at the time alerted controllers or pilots of the hazardous wind-shear conditions. This is due to the fact that adverse conditions were not experienced at the surface as a result of a cold pool decoupling surface conditions from those aloft. For more information on uncontrolled descent of the 767, see Isaminger et al. (2003).

The TWINDS analysis utilizing inputs from the DIX and OKX NEXRADs and EWR and JFK TDWRs was used to construct a headwind-tailwind profile along the approach path of the 767. This profile is illustrated in the image that encompasses the time vs. height plot of the 767 (right-side image of Figure 3-12). For information regarding the generation of path-based shear profiles see Allan et al. (2004) and Bieringer et al. (2004). In the Figure 3-12 image, colored contours bound isopleths of headwinds (increasing in velocity with darkening shades of gray) and tailwinds (increasing in velocity with darkening shades of red). Aircraft altitude over time is, once again, denoted by the blue line. Notice the accumulated loss of roughly 15 m s^{-1} (30 kts) occurring between 00:57:00Z and 00:58:30Z. Pilot response and this accumulated loss is what led to the uncontrolled descent of 1200 ft that began shortly after 00:58:00Z.

Low-elevation Doppler velocity scans from the TDWRs and NEXRADs show that EWR and JFK TDWRs are properly positioned to best capture the near-terminal wind-shear event (Figure 3-13). Inbound and outbound velocities are scaled between ±30 m s^{-1} as noted by the color bars to the far right of the figure. Aircraft position is plotted in red for reference. The gradient of the shear boundary is best captured by EWR with gate-to-gate shear being resolved along the boundary of the gradient (notice the green inbound velocities embedded in gold and pink outbound velocities north and west of JFK). In comparison to the TDWR, the DIX and OKX NEXRADs are not well positioned to capture the near-terminal event. A weak velocity signature is visible in the OKX 0.5° scan and no signature is discernable in the DIX scan. Other NEXRAD scans from different times or elevations angles revealed no velocity signature of the event. Lack of a velocity signature will have a detrimental affect on the no-TDWR TWINDS analysis of this operationally hazardous event.

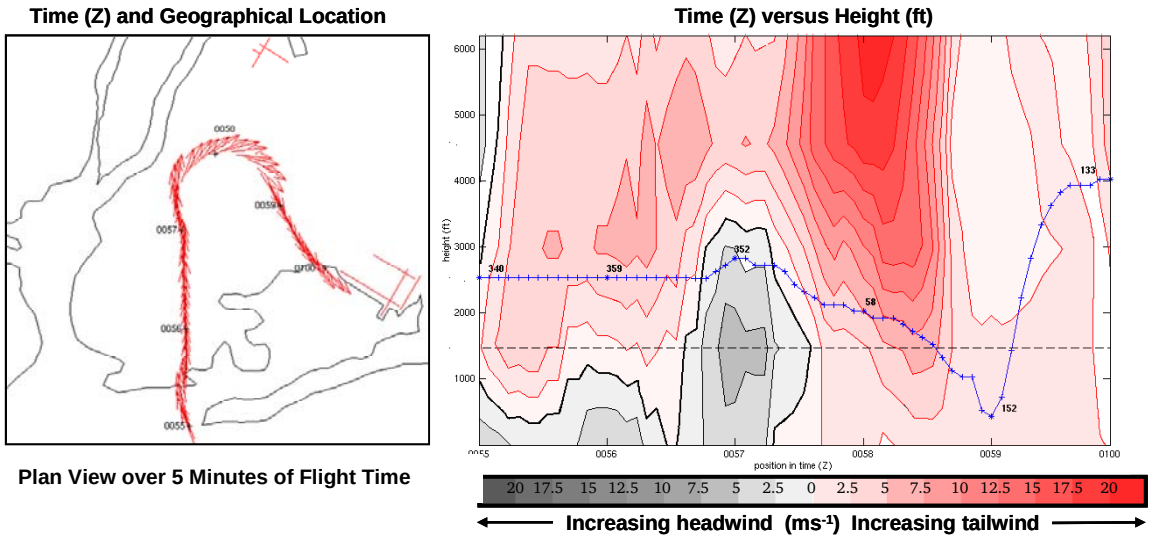

Figure 3-12. Uncontrolled descent of a Boeing 767 passenger flight on final approach to JFK. Red vectors in the far left diagram provide the instantaneous headings used in the creation of the headwind-tailwind profile seen in the far right plot. Colored contours in the far right plot bound isopleths of headwinds (increasing in velocity with darkening shades of gray) and tailwinds (increasing in velocity with darkening shades of red). Aircraft altitude over time is denoted by the blue line. Notice the accumulated loss of roughly 15 m s-1 (30 kts) occurring between 00:57:00Z and 00:58:30Z. The uncontrolled decent of 1200 ft in less than 1 minute began shortly after 00:58:00Z.

Figure 3-14 shows the TWINDS analyses comparisons at the layer and time nearest to the uncontrolled descent of the 767 (00:55:00Z analysis at 950 mb (~1800 ft)). To the left is the analysis with TDWRs not utilized as radar input, to the right is the analysis utilizing the EWR and JFK TDWRs. Magenta wind vectors sit atop a centered divergence field, which is used to indicate where large discontinuities in the wind field exist, the result of speed shear and wind direction changes. The divergence field is scaled between ±4 m s^{-1} km^{-1}, where deep shades of blue indicate strong convergence and deep shades of red indicate strong divergent flow. While the vertical component of the winds is not computed utilizing TWINDS, through conservation of mass strong divergence and convergence is directly related to vertical velocities on the convective scale (m s^{-1} to 10s of m s^{-1}).

Revealed by the side-by-side comparison of the two TWINDS analyses is that the shear boundary that resulted in the uncontrolled decent of the 767 is in no way resolved by the analysis that excludes TDWR as input (left-side image of Figure 3-14). The right-side image reveals that the TWINDS analysis utilizing TDWR data properly reveals the gradient and severity of the shear boundary. It also reveals the convergence/divergence couplet signatures commonly associated with mesoscale buoyancy waves, and the presence of divergences and convergences can be directly related to velocities that would cause the type of operational hazard that was unfortunately experienced by the 767 pilots on 29 April 2002.

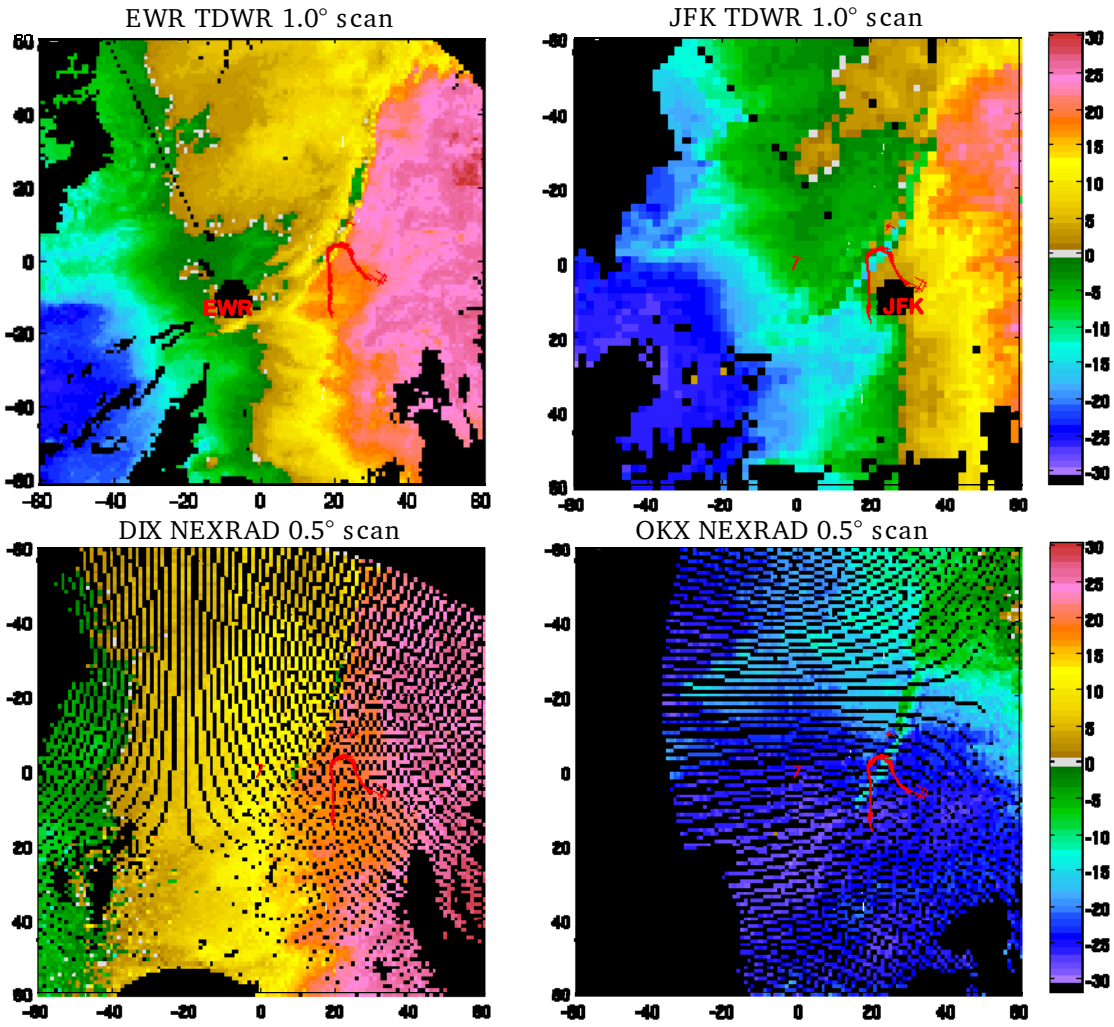

Figure 3-13. Low-tilt radial Doppler velocity scans (m s^{-1}) from the four radars used in the TWINDS analysis over the New York airports. Plotted scans are scaled between inbound and outbound velocities of 30 m s^{-1}. Scan times are those that correspond closest to the time of the 767's uncontrolled descent. The aircraft position relative to each scan is indicated by the red line just right of center. The 1.0° scans from the EWR and JFK TDWRs (upper left and upper right) show that the TDWRs resolve the gradient of this near-terminal event much better than the DIX and OKX NEXRADs (lower left and lower right).

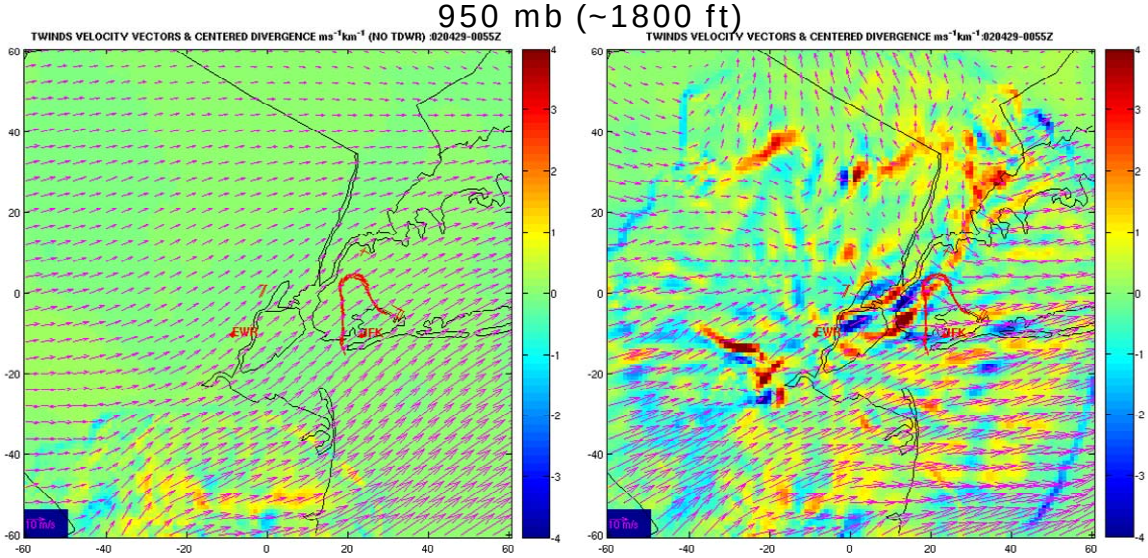

Figure 3-14. TWINDS comparisons at the layer and time nearest to the uncontrolled descent (00:55:00Z analysis at 950 mb (~1800 ft)). Left is the analysis with TDWR data not utilized for input; right is the analysis utilizing the EWR and JFK TDWRs. Magenta wind vectors sit atop a centered divergence field, deep blue indicates strong convergence and deep red indicates strong divergent flow, both indicative of vertical velocities on the convective scale (m s^{-1} to 10s of m s^{-1}).

4. CONCLUSIONS

Decommissioning the TDWR will clearly have a significantly negative impact on terminal-area safety. Even with the addition of the WSP to ASR-9s closest to the original TDWR sites, two airports would lose all wind-shear radar coverage, while 13 airports (including 7 of the top-20 busiest in the U.S.) would be left without acceptable microburst alert capability. Even if NEXRAD data were to be used for gust-front detection and tracking, 61% of airports would lose adequate coverage in the 10-60 km range.

The ITWS TWINDS errors will increase dramatically at low altitude in the terminal area, which will surely degrade the substantial delay reduction benefits currently reaped through the use of that product. The NEXRADs on their own are spaced too far apart to provide dual-Doppler coverage at low altitude over any TDWR airport. The degradation in wind estimate quality will be worst at some of the busiest terminal clusters such as New York, Chicago, Dallas, Houston, Miami, and Washington, D.C., where there are two or more TDWRs contributing to the TWINDS domain.

The fundamental reasons why the functionality of the TDWR is so hard to replace are that (1) ASR-9s were not designed for weather surveillance and (2) NEXRADs were not sited for terminal surveillance. The WSP does an excellent job of wringing every possible bit of weather information out of the ASR-9, but an add-on processing system cannot substantially increase the sensitivity of the radar or turn a fan beam into a pencil beam. Moving around NEXRADs in order to better cover airports that would be losing their TDWRs does not appear to be a feasible alternative because of the inability of the NEXRAD to satisfy existing microburst detection and reporting requirements.

Although we focused on the ITWS TWINDS product in this report, there are other delay reduction tools that benefit from the TDWR's ability to see low with good vertical resolution around the airport. Winter precipitation and stratiform rain can be confined to low altitudes that NEXRADs may overshoot in the terminal area. Weather forecasts need boundary layer wind measurements for accurate convective initiation modeling. Potential future uses include wind-field diagnosis to support adaptive wake vortex separation procedures and improved lightning warnings that support more efficient airport ramp operations. Also there are users besides the FAA that utilize TDWR data. For example, in 2005, the NWS began national deployment of the Supplemental Product Generator (SPG), which allows data from the TDWR to be fully integrated with NEXRAD data and other weather data on the Advanced Weather Interactive Processing System (AWIPS) (Istok et al. 2005).

APPENDIX A
COMPLETE RESULTS TABLES

TABLE A-1

TDWR Airports and Closest ASR-9s and NEXRADs

TDWR Airport	ASR-9	NEXRAD	Distance to Airport (km)			Min. Obs. Height (ft)		
			TDWR	ASR-9	NEXRAD	TDWR	ASR-9	NEXRAD
ADW	ADW	LWX	13.0	0.2	56.1	99	6	681
ATL	ATL	FFC	15.3	1.3	33.3	353	70	145
BNA	BNA	OHX	16.1	0.3	17.1	270	27	119
BOS	BOS	BOX	23.6	1.7	46.7	353	37	618
BWI	BWI	LWX	10.1	1.4	73.5	171	34	1252
CLE	CLE	CLE	18.9	0.9	0.9	209	82	54
CLT	CLT	GSP	14.7	0.4	122.1	167	36	3186
CMH	CMH	ILN	15.1	1.1	102.3	378	88	2361
CVG	CVG	ILN	18.0	0.8	83.7	203	24	1613
DAL	QZB	FWX	14.0	15.6	52.1	173	223	786
DAY	DAY	ILN	15.6	2.0	63.5	57	68	924
DCA	DCA	LWX	12.3	0.9	83.7	359	17	657
DEN	DVX	FTG	19.5	3.9	13.8	349	0	201
DFW	DFW	FWS	21.7	2.9	43.7	70	90	510
DTW	DTW	DTX	17.5	2.2	55.0	182	122	1140
EWR	EWR	DIX	14.0	2.5	85.3	156	81	1602
FLL	FLL	AMX	20.7	0.5	57.5	193	47	725
HOU	HOU	HGX	14.8	3.1	27.3	113	54	198
IAD	IAD	LWX	16.7	1.5	3.9	214	48	44
IAH	IAH	HGX	23.5	1.9	62.2	262	48	751
ICT	ICT	ICT	15.9	0.8	1.0	66	32	51
IND	IND	IND	15.1	1.7	1.6	97	92	79
JFK	JFK	OKX	10.3	1.1	81.2	97	78	1444
LAS	LAS	ESX	14.8	2.1	48.2	0	0	3201
LGA*	JFK	OKX	20.9	17.7	85.6	199	130	1577
MCI	MCI	EAX	22.4	2.0	66.7	176	2	909
MCO	MCO	MLB	9.6	3.9	73.2	91	61	1038

TDWR Airport	ASR-9	NEXRAD	Distance to Airport (km)			Min. Obs. Height (ft)		
			TDWR	ASR-9	NEXRAD	TDWR	ASR-9	NEXRAD
MDW	QXM	LOT	15.1	18.3	34.2	187	203	351
MEM	MEM	NQA	16.3	3.3	34.8	194	61	313
MIA	MIA	AMX	20.5	0.5	23.7	191	41	196
MKE	MKE	MKX	18.7	1.9	53.4	278	82	835
MSP	MSP	MPX	22.5	1.3	27.8	378	94	395
MSY	MSY	LIX	14.4	0.6	56.4	134	25	775
OKC	OKC	CRI	15.4	2.3	21.5	10	28	93
ORD	ORD	LOT	20.5	2.0	44.2	156	84	454
PBI	FLL	AMX	17.7	68.4	123.0	176	940	2999
PHL	PHL	DIX	17.0	2.6	71.5	173	57	1165
PHX	PHX	IWA	14.1	1.4	35.6	0	89	521
PIT	PIT	PBZ	21.5	3.3	4.6	265	90	51
RDU	RDU	RAX	16.0	1.0	35.8	130	48	258
SDF	SDF	LVX	18.0	1.6	28.7	293	58	475
SJU	MIA	JUA	19.2	1682.8	36.7	219	5.47E5	3195
SLC	SLC	MTX	20.3	2.6	65.9	151	26	3189
STL	STL	LSX	12.9	1.2	28.6	75	58	260
TPA	TPA	TBW	12.9	1.8	32.6	101	57	286
TUL	TUL	INX	15.2	3.1	29.2	193	5	222

* Closest TDWR to LGA is JFK.

TABLE A-2

Visibility for Microburst (Top) and Gust Front (Bottom) by Airport

Airport	Radius Around Airport					
	0-10 km			10-60 km		
	TDWR	ASR-9	NEXRAD	TDWR	ASR-9	NEXRAD
ADW	100 98	94 89	40 95	77 97	31 3	36 59
ATL	100 98	93 88	100 99	76 97	28 3	61 83
BNA	100 98	93 88	100 96	41 77	26 3	73 91
BOS	100 99	88 84	59 98	52 95	24 2	37 65
BWI	100 97	93 88	0 42	71 97	24 2	17 39
CLE	100 98	94 89	99 92	65 97	24 2	77 84
CLT	100 98	93 88	0 0	70 97	29 3	0 3
CMH	100 98	93 88	0 0	45 96	27 3	0 14
CVG	100 98	94 89	0 11	66 97	30 3	8 30
DAL	100 98	78 56	9 95	70 97	26 6	30 58
DAY	100 98	93 88	0 79	79 98	28 3	28 50
DCA	100 98	35 32	46 99	45 97	5 0	32 67
DEN	95 99	41 87	93 95	31 80	0 3	40 82
DFW	100 99	93 89	92 99	73 98	27 3	42 70
DTW	100 98	93 89	0 80	68 97	27 3	9 47

Airport	Radius Around Airport					
	0 - 10 km			10 – 60 km		
	TDWR	ASR-9	NEXRAD	TDWR	ASR-9	NEXRAD
EWR	100 98	87 84	0 11	55 75	18 1	10 29
FLL	100 99	93 88	28 93	66 97	29 3	35 57
HOU	100 98	93 89	100 99	75 97	28 3	63 87
IAD	100 98	94 89	99 92	49 80	26 3	71 78
IAH	100 99	93 88	23 87	60 96	29 3	35 54
ICT	100 98	94 89	98 91	78 98	29 3	85 91
IND	100 98	93 88	98 92	75 97	27 3	81 91
JFK	100 97	93 89	0 22	79 97	27 3	13 33
LAS	98 98	30 62	0 0	8 9	0 0	0 0
LGA	100 99	77 49	0 12	66 97	28 7	11 30
MCI	100 99	94 89	0 76	67 97	31 4	29 49
MCO	100 97	93 89	0 57	80 97	28 3	26 44
MDW	100 98	73 44	99 99	68 97	27 7	52 79
MEM	100 98	93 89	99 100	67 97	28 3	54 80
MIA	100 99	94 89	100 98	66 97	29 3	65 88
MKE	100 98	93 89	0 93	59 97	27 3	28 56
MSP	100 99	93 89	99 99	49 95	27 3	48 83

Airport	Radius Around Airport					
	0 – 10 km			10 – 60 km		
	TDWR	ASR-9	NEXRAD	TDWR	ASR-9	NEXRAD
MSY	100 98	93 89	14 92	73 97	30 3	32 56
OKC	100 98	93 88	100 97	80 98	29 3	73 91
ORD	100 99	93 89	98 99	69 97	27 3	46 71
PBI	100 98	0 0	0 0	69 98	10 3	0 5
PHL	100 98	93 88	0 51	69 97	27 3	20 42
PHX	91 91	38 82	59 99	30 41	0 0	22 51
PIT	100 99	93 89	99 92	60 97	27 3	85 91
RDU	100 98	91 87	99 100	73 97	28 3	58 81
SDF	100 98	88 84	99 99	57 97	23 2	41 80
SJU	100 99	0 0	0 0	43 61	0 0	0 0
SLC	85 86	38 81	0 0	19 28	0 0	0 0
STL	100 98	94 89	100 99	79 97	28 3	59 85
TPA	100 98	93 89	99 99	77 97	28 3	56 82
TUL	100 98	93 88	100 99	68 97	26 2	61 85

TABLE A-3
Mean Vector Wind Error (m s^{-1}) at 2nd Lowest (Top) and Lowest (Bottom) Levels

Airport	Without TDWR		With TDWR		Difference	
	20x20 km	60x60 km	20x20 km	60x60 km	20x20 km	60x60 km
ADW	5.3 7.1	5.9 7.1	0.7 1.72	0.7 4.9	4.7 5.4	5.2 2.2
ATL	5.0 7.1	5.2 6.9	1.3 6.4	1.6 6.6	3.8 0.7	3.5 0.3
BNA	5.0 5.0	5.0 5.1	1.7 1.7	1.8 2.0	3.3 3.3	3.3 3.2
BOS	5.1 6.6	5.2 6.4	1.9 4.2	2.6 4.3	3.1 2.4	2.6 2.1
BWI	6.6 7.1	6.3 7.1	1.3 5.0	1.9 4.9	5.3 2.0	4.5 2.1
CLE	5.1 5.1	5.2 5.3	1.9 1.9	2.5 3.0	3.2 3.2	2.8 2.3
CLT	7.1 7.1	7.1 7.1	5.0 5.0	5.0 5.3	2.0 2.0	2.0 1.8
CMH	7.1 7.1	7.0 7.1	5.0 5.0	5.0 5.5	2.0 2.0	2.0 1.6
CVG	7.1 7.1	6.7 7.1	5.0 5.1	4.5 6.0	2.0 2.0	2.2 1.1
DAL	5.1 5.8	5.2 6.1	0.8 1.0	1.1 1.5	4.3 4.9	4.1 4.7
DAY	6.2 7.1	6.2 7.1	3.6 6.1	3.8 6.6	2.6 0.9	2.4 0.5
DCA	5.0 5.9	5.1 6.2	0.6 1.8	0.6 1.3	4.5 4.1	4.5 4.8
DEN	5.0 5.0	5.1 6.0	3.3 3.4	3.6 5.0	1.7 1.6	1.5 1.0
DFW	5.0 5.6	5.1 6.1	1.3 1.4	1.1 1.4	3.7 4.1	4.0 4.7
DTW	5.1 7.0	5.4 6.5	1.3 4.9	2.2 4.3	3.8 2.1	3.2 2.2
EWR	7.1 7.1	6.6 7.1	1.0 1.0	1.8 3.0	6.0 6.0	4.8 4.1

Airport	Without TDWR		With TDWR		Difference	
	20x20 km	60x60 km	20x20 km	60x60 km	20x20 km	60x60 km
FLL	5.1 7.1	5.6 6.7	0.7 4.3	1.0 4.1	4.4 2.7	4.6 2.6
HOU	5.0 5.1	5.0 5.8	1.3 2.0	1.2 2.9	3.7 3.1	3.8 2.9
IAD	5.0 5.1	5.2 6.6	0.9 3.6	1.6 6.0	4.1 1.5	3.6 0.6
IAH	5.3 7.1	5.9 6.9	1.0 5.0	2.1 5.2	4.3 2.0	3.8 1.7
ICT	5.0 5.0	5.0 5.0	1.6 1.6	2.1 2.2	3.4 3.4	2.9 2.8
IND	5.0 5.0	5.0 5.1	1.7 1.7	2.3 2.7	3.3 3.3	2.8 2.4
JFK	6.9 7.1	6.2 7.1	2.3 3.4	1.6 3.4	4.5 3.7	4.6 3.7
LAS	5.1 6.9	5.2 6.5	1.1 4.7	4.2 5.8	4.0 2.1	1.0 0.7
LGA	7.1 7.1	6.5 7.1	0.9 2.4	1.5 3.8	6.1 4.6	5.0 3.2
MCI	6.6 7.1	6.4 7.1	4.6 7.0	4.2 6.8	2.0 0.1	2.2 0.3
MCO	6.4 7.1	6.3 7.1	3.9 5.0	3.8 5.3	2.5 2.0	2.5 1.8
MDW	5.0 5.1	5.1 5.7	0.7 0.7	1.0 1.2	4.3 4.3	4.0 4.5
MEM	5.0 7.1	5.3 7.0	2.3 6.8	1.8 6.8	2.8 0.3	3.5 0.2
MIA	5.0 5.0	5.0 5.5	0.7 0.9	0.9 2.1	4.3 4.2	4.1 3.4
MKE	5.1 7.1	5.5 6.6	1.3 5.0	2.4 4.5	3.8 2.0	3.0 2.1
MSP	5.0 5.5	5.1 6.0	2.4 3.1	1.3 4.7	2.7 2.4	3.8 1.4
MSY	5.1 7.1	5.5 6.7	1.6 5.0	2.4 4.7	3.5 2.0	3.1 2.0
OKC	5.0 5.0	5.0 5.2	4.2 4.2	3.7 3.8	0.9 0.9	1.3 1.4

Airport	Without TDWR		With TDWR		Difference	
	20x20 km	60x60 km	20x20 km	60x60 km	20x20 km	60x60 km
ORD	5.0	5.1	1.2	1.3	3.8	3.8
	6.0	6.2	2.4	3	3.6	3.2
PBI	7.1	7.1	1.3	2.8	5.8	4.3
	7.1	7.1	5.0	5.1	2.0	2.0
PHL	6.0	6.1	3.8	3.4	2.2	2.7
	7.1	7.1	5.0	5.3	2.0	1.7
PHX	5.1	5.3	2.3	3.5	2.8	1.8
	5.1	5.6	2.4	3.9	2.8	1.7
PIT	5.0	5.0	1.6	1.8	3.5	3.3
	5.0	5.0	1.6	1.9	3.5	3.2
RDU	5.0	5.1	1.0	1.5	4.1	3.6
	5.1	5.4	1.0	2.0	4.0	3.4
SDF	5.0	5.0	0.9	1.6	4.1	3.5
	5.0	5.2	0.9	2.0	4.1	3.3
SJU	5.0	5.1	0.9	2.7	4.1	2.4
	5.5	6.0	1.8	4.3	3.7	1.7
SLC	5.1	5.7	2.0	4.1	3.1	1.5
	7.1	6.6	5.4	5.5	1.7	1.1
STL	5.0	5.0	1.6	2.2	3.4	2.9
	5.0	5.5	1.6	2.6	3.4	2.9
TEB	7.1	7.0	0.9	1.9	6.2	5.1
	7.1	7.1	1.3	4.2	5.7	2.9
TPA	5.0	5.1	2.8	2.5	2.2	2.6
	5.2	5.9	2.9	3.3	2.2	2.6
TUL	5.0	5.0	1.0	1.8	4.0	3.2
	5.1	5.7	1.1	2.7	4.0	3.0

APPENDIX B
COMPUTATION OF WIND-SHEAR VISIBILITY

The radar visibility of wind-shear phenomena is dependent on three factors: clear line of sight (terrain blockage), signal-to-noise ratio (SNR), and signal-to-clutter ratio (SCR). To compute the average visibility over a specified area, one can take the measured reflectivity probability distribution function (PDF) of the phenomenon and integrate over it and over the area of interest, using the minimum detectable reflectivity at a given point as the lower limit of the first integration. Ideally, the SCR factor would be included in this lower limit, but that would require knowledge of the areal distribution of ground clutter at all airports for all radars, which we do not have. Instead we will compute the visibility due to SNR and SCR limitations separately (the latter using an averaged clutter reflectivity PDF) and calculate a joint visibility using reasonable assumptions.

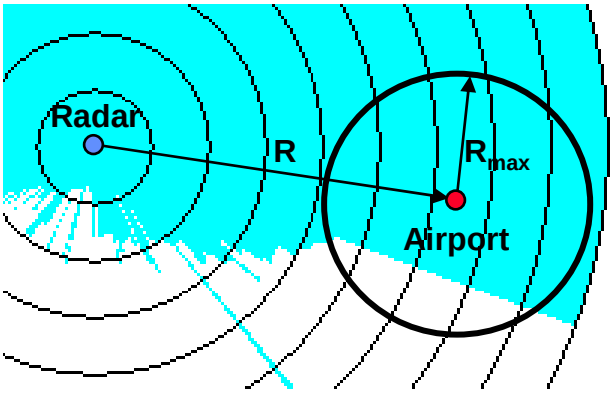

Figure B-1. Geometry used for wind-shear visibility computation.

Figure B-1 shows the geometry used in the visibility calculation. R is the distance from the radar to the center of the airport and R_{max} is the radius around the airport for which we compute the visibility. The light blue shading indicates clear light of sight from the radar. The visibility due to SNR limitations is computed as

$$F_{SNR}(R) = \frac{1}{\pi R_{max}^2} \int_{R-R_{max}}^{R+R_{max}} \int_{Z_{eff}(r)}^{\infty} 2r \cos^{-1}\left(\frac{r^2 + R^2 - R_{max}^2}{2Rr}\right) p(Z_W)\, dZ_W\, dr \qquad R \geq R_{max} \quad \text{(B-1)}$$

$$= \frac{1}{\pi R_{max}^2}\left[\begin{array}{l} \int_{0}^{R_{max}-R} \int_{Z_{eff}(r)}^{\infty} 2\pi r\, p(Z_W)\, dZ_W\, dr + \\ \int_{R_{max}-R}^{R+R_{max}} \int_{Z_{eff}(r)}^{\infty} 2r \cos^{-1}\left(\frac{r^2 + R^2 - R_{max}^2}{2Rr}\right) p(Z_W)\, dZ_W\, dr \end{array}\right] \qquad R < R_{max} \quad \text{(B-2)}$$

where Z_W is the wind-shear reflectivity, $p(Z_W)$ is its PDF, and Z_{eff} is the effective minimum detectable reflectivity given by

$$Z_{\text{eff}}(r) = \left[Z_{\min}(r) + SNR_{\text{CPI}} + SNR_{\text{thres}} - BL(r)\right]\delta_{\text{LOS}}(r) \tag{B-3}$$

where $Z_{\min}$ is the classical minimum detectable reflectivity in dBZ, SNR_{CPI} is the adjustment required based on coherent processing interval (CPI) and pulse repetition frequency (PRF) differences in dB, SNR_{thres} is the extra SNR needed for accurate velocity-shear estimation in dB, BL is the two-way beam-filling loss in dB, and δ_{LOS} is the line-of-sight terrain blockage function, which is 1 for clear and ∞ for blocked sight. The variable r is the range from the radar.

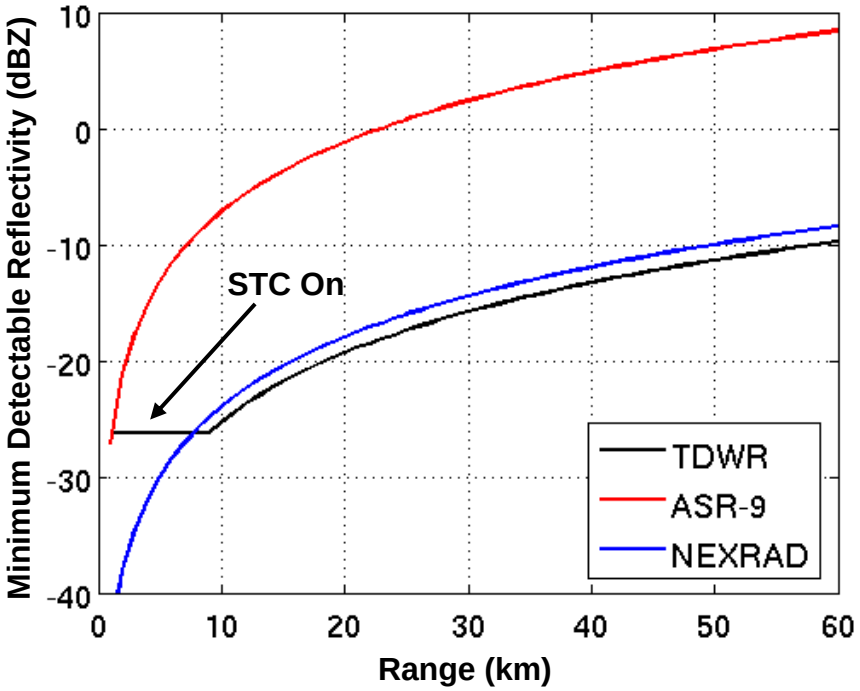

Figure B-2. Classical minimum detectable reflectivity vs. range for the TDWR, ASR-9 WSP, and NEXRAD.

Figure B-2 shows $Z_{\min}$ for all three radars. The TDWR utilizes a sensitivity time control (STC) function at close range to avoid receiver saturation due to strong ground clutter returns. The STC function on the ASR-9 is site dependent and only used on specific radials, so we ignore it. The NEXRAD does not use STC.

Because the ASR-9 is used to monitor air traffic its scans must be repeated quickly, which requires a fast antenna rotation rate. The CPI, correspondingly, must be short, which means a small number of pulses averaged per dwell. This leads to a larger error in the reflectivity and velocity estimates. Velocity estimate errors based on typical signal processing parameters for the three radars are shown in Figure B-3. Errors were computed based on a perturbation analysis by Zrnić (1977). The arrows in the figure point out that to obtain the same error level, the ASR-9 needs a SNR few dBs larger than the TDWR in the 0-dB SNR vicinity. The NEXRAD velocity estimate error is also slightly worse than the TDWR, which is due to its generally lower PRF required for longer unambiguous range. Thus we assign values of 0, -2, and -3 dB to SNR_{CPI} for the ASR-9 WSP, NEXRAD, and TDWR.

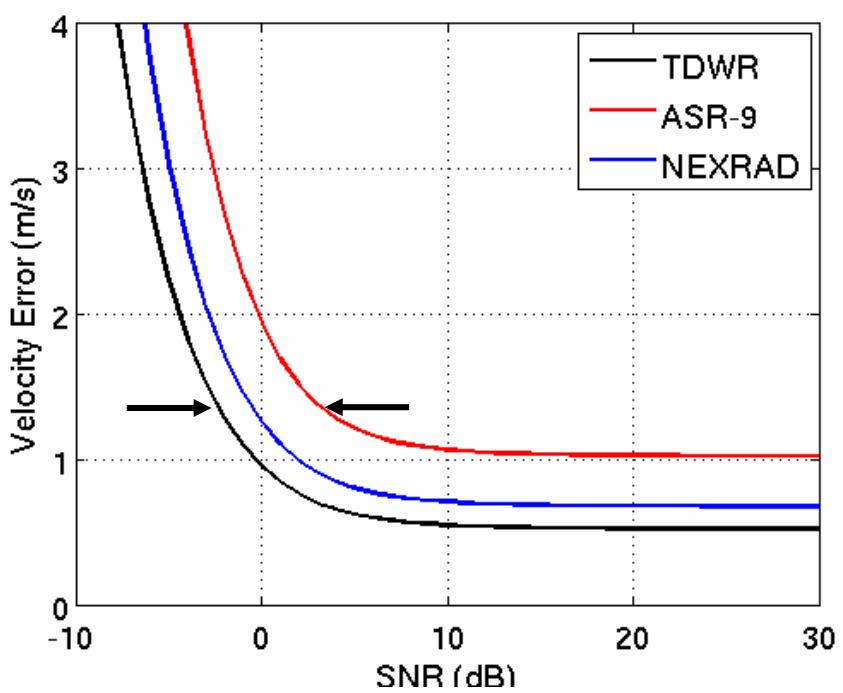

Figure B-3. Typical velocity estimate error vs. SNR for the TDWR, ASR-9 WSP, and NEXRAD.

The classical minimum detectable weather reflectivity metrics assume volume-filled scattering. However, for altitude-limited phenomena this assumption is not correct. Reflectivity signatures from microburst and gust-front outflows are limited to heights near the surface, so only the lower part of the antenna beam may be filled with these scatterers. Because of the Earth's curvature, this filled fraction decreases further with range until, at some point, no scatterers are present within the beam. This "beam-filling loss" adjustment factor grows larger with the elevation beamwidth, which means that the TDWR is least affected and the ASR-9 is most affected. Figure B-4 shows the two-way beam-filling loss (*BL*) for all three radars with assumed scatterer ceilings of 200 m (microburst outflow) and 500 m (gust-front outflow). These values were determined from low-altitude wind-shear morphology statistics collected with the TDWR testbed (Biron and Isaminger 1991; Klingle-Wilson and Donovan 1991). The theoretical elevation beam patterns for the ASR-9 were used in computing the beam-filling loss (Weber and Moser 1987) while Gaussian functions were used to approximate the pencil-beam patterns of the TDWR and NEXRAD. Microburst detection with the ASR-9 WSP requires adequate SNR in both high and low beams, so the worse case (high beam) loss is assumed. For gust-front detection by the WSP only the low beam is used.

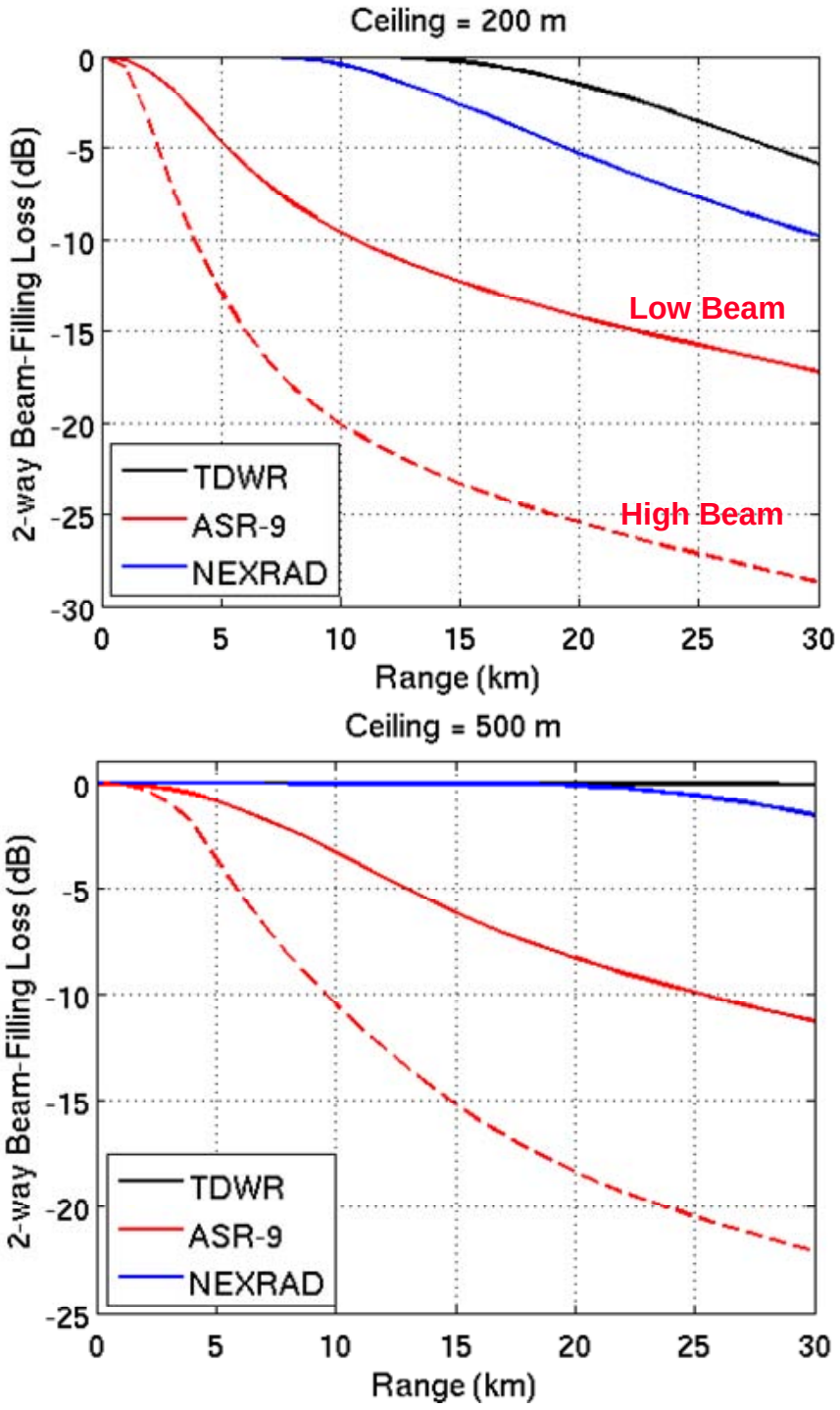

Figure B-4. Two-way beam-filling loss vs. range for an assumed target ceiling of 200 m (top) and 500 m (bottom).

For microburst detection, very accurate velocity estimation is required, while for gust-front detection the primary indicator is a reflectivity thin line. Thus, microburst detection needs a higher SNR margin than for gust fronts. We use SNR_{thres} = 6 and 3 dB for the microburst and gust-front cases (Weber and Troxel 1994).

As for the wind-shear reflectivity PDF, $p(Z_W)$, we use data collected previously by the TDWR testbed radar (Weber and Troxel 1994). Microburst outflow reflectivities have very different distributions at wet vs. dry sites (Figure B-5, top). Of the 47 TDWR-serviced airports only four are categorized as "dry": Denver, Las Vegas, Phoenix, and Salt Lake City. Gust-front reflectivities do not differ so much with location, so we use a nationally averaged PDF (Figure B-5, bottom).

We compute the wind-shear visibility under clutter-limited conditions by

$$F_{\text{SCR}} = \int_0^{\infty} p(Z_C) \int_{Z_{\text{lim}}}^{\infty} p(Z_W) dZ_C dZ_W \tag{B-4}$$

where Z_C is the clutter reflectivity, $p(Z_C)$ is its PDF, and Z_{lim} is the effective minimum detectable reflectivity over clutter given by

$$Z_{\text{lim}} = Z_C - S - S_D + SCR_{\text{thres}} \tag{B-5}$$

where S is the clutter suppression capability of the radar in dB (Table 4), SCR_{thres} = 10 dB is the required SCR margin for wind-shear detection (Weber and Troxel 1994), and S_D is the difference in SCR seen by radars with different beamwidths and wavelengths given by

$$S_D = 10 \log\left(\frac{\Delta\theta \lambda_{\text{ref}}^4}{\Delta\theta_{\text{ref}} \lambda^4} \right) \tag{B-6}$$

where $\Delta\theta$ is the elevation beamwidth, λ is the wavelength, and the subscript "ref" labels the reference radar. The clutter reflectivity data that we used were collected by the ASR-9 testbed radar, so the ASR-9 is the reference and we get S_D = 0, 3, and -7 dB for the ASR-9 WSP, TDWR, and NEXRAD.

Figure B-6 shows the measured ground clutter reflectivity distributions (in dBZ) for two sites considered to be severe and moderate clutter environments (Weber and Troxel 1994). For this study we take the average of these two distributions.

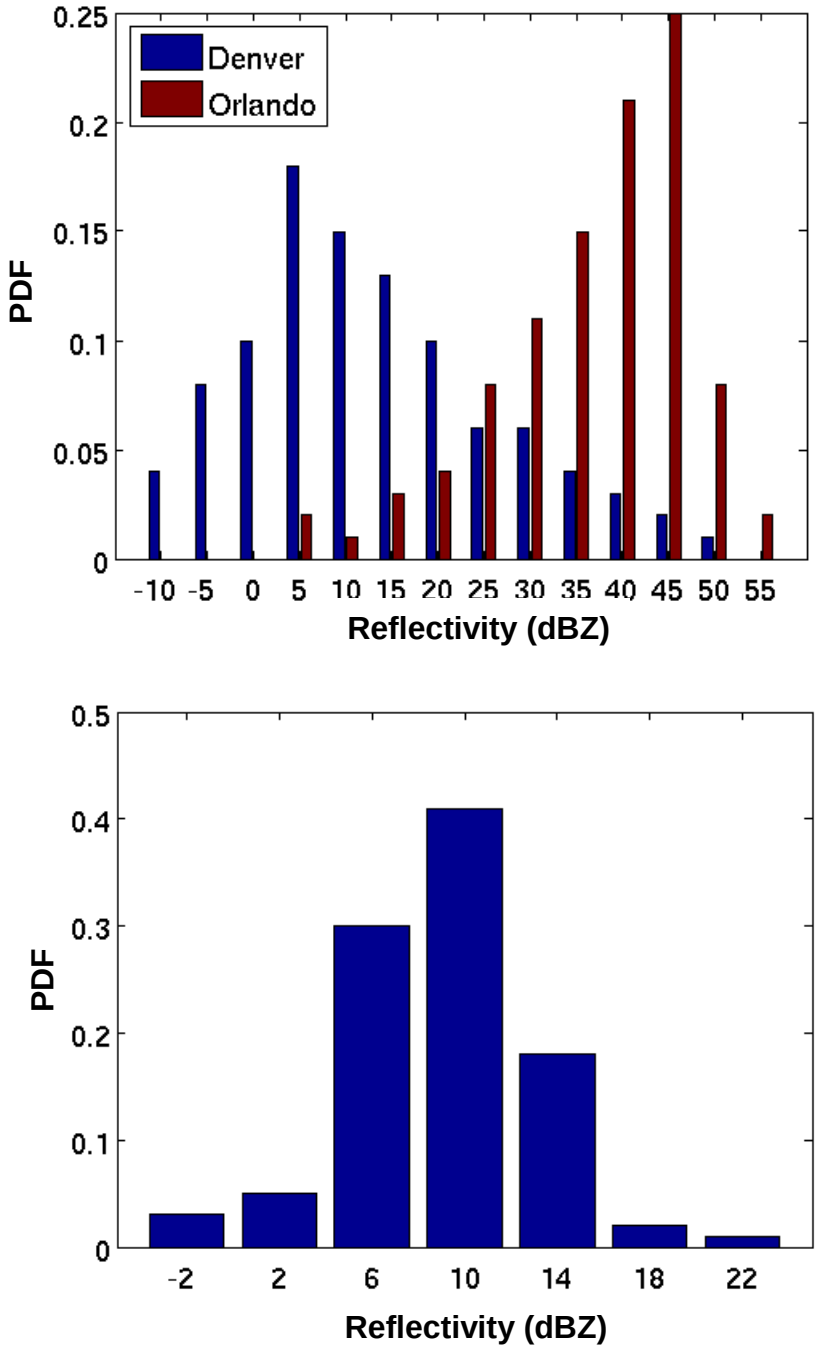

Figure B-5. PDFs for microburst outflow reflectivity (top) at a dry site (blue) and wet site (red), and nationally averaged gust front reflectivity (bottom).

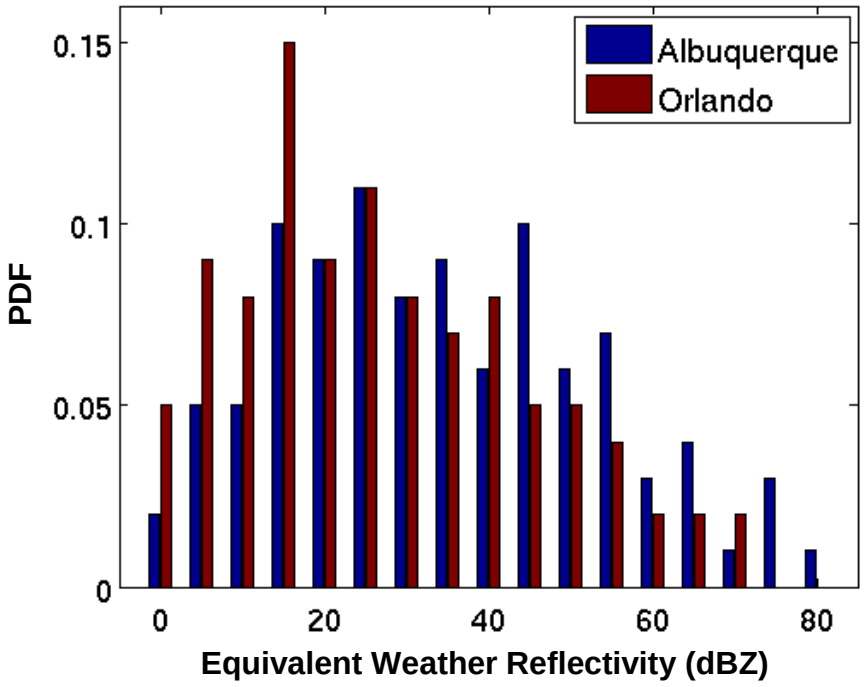

Figure B-6. Measured probability distribution functions of ground clutter reflectivity from two sites.

Finally, we combine the results from A-1, A-2, and A-4 for a joint visibility measure (adapted from Weber (1999))

$$F_{\text{vis}}(R) = F_{\text{SNR}} + f_C\left[F_{\text{SCR}} - \frac{1}{2} - \frac{1}{2}\max(F_{\text{SNR}}, F_{\text{SCR}})\right] \tag{B-7}$$

where

$$f_C(R) = Ae^{-\frac{R^2}{2\sigma^2}} \tag{B-8}$$

is the fraction of resolution cells that is clutter limited. We take A = 0.47 (Weber 1999) and σ = 15 km. As the distance from the radar to the airport (and, thus, the distance to the area of interest) increases, the fraction of clutter-limited cases decreases.

APPENDIX C
COMPUTATION OF TWINDS OUTPUT WIND ERROR

The ITWS TWINDS algorithm takes velocity data input from the RUC numerical weather prediction program, TDWRs, NEXRADs, meteorological ground stations, and aircraft reports. It uses a cascade-of-scales scheme to take full advantage of the different resolution scales of the input data. The output consists of horizontal velocities at 1-km resolution on pressure surfaces spaced 25 mb apart from 1000 mb (360 ft MSL) to 100 mb (53,000 ft MSL) (Cole and Wilson 1994).

Our aim here is to capture the basic change in output wind estimate quality with and without TDWR data. The purpose is not to accurately quantify the absolute error values at particular locations within the TWINDS domain. As such, we make some simplifying assumptions in our calculations.

1. Exclude aircraft and ground-station data. These data are spatially sparse, with the former with data points mainly at high altitude and the latter confined to ground level near the terminal (and only available at certain airports).
2. Work on the fine-scale grid only and ignore displacement errors. This essentially means that all input data points are treated equally in terms of the measurement scales they represent.
3. Assume a constant wind error value of 5 m s^{-1} (7.1 m s^{-1} vector wind error) for the RUC data. This is a typical value taken from Cole et al. (2000).
4. Assume a constant weather reflectivity of 10 dBZ and a spectral width of 3 m s^{-1}. This reflectivity is a reasonable background value that provides enough SNR for velocity estimation at the ranges of interest. The spectral width is also a reasonable value; in any case, the results are not very sensitive to its variation.
5. Ignore clutter effects. Lacking a clutter distribution map for every site and radar, we simply omit this factor.

At the heart of TWINDS is the matrix equation

$$\mathbf{u}_{\mathbf{est}} = \left(\mathbf{A}^{\mathbf{T}}\mathbf{C}^{-1}\mathbf{A}\right)^{-1}\mathbf{A}^{\mathbf{T}}\mathbf{C}^{-1}\mathbf{u}_{\mathbf{obs}} \qquad \text{(C-1)}$$

where $\mathbf{u}_{\mathbf{obs}}$ is the input wind data vector, $\mathbf{u}_{\mathbf{est}}$ is the output wind data vector, $\mathbf{A}$ is a matrix containing geometric factors, $\mathbf{C}$ is a matrix containing the input data variances, and T denotes transpose. The output errors can be obtained from the covariance matrix, $(\mathbf{A}^{\mathbf{T}}\mathbf{C}^{-1}\mathbf{A})^{-1}$.

With the above assumptions, we compute the output vector wind error field for a 120 x 120 km domain around each TDWR airport on the first two pressure levels above the terminal ground level. The variances of the TDWR and NEXRAD velocity data are computed using the perturbation analysis equation of Zrnić (1977) (see Figure B-3). As for the visibility calculation, the effects of terrain blockage, beam-filling loss, and CPI differences are included. The TDWR and NEXRAD data that are used as input for each terminal area are shown in Table C-1. This information corresponds to actual ITWS radar usage.

TABLE C-1

TDWR and NEXRAD Input to TWINDS Error Calculation

TDWR Airport	TDWR(s)	NEXRAD(s)
ADW	ADW/BWI/DCA/IAD	FCX/LWX
ATL	ATL	FFC
BNA	BNA	OHX
BOS	BOS	BOX
BWI	ADW/BWI/DCA/IAD	FCX/LWX
CLE	CLE	CLE
CLT	CLT	GSP
CMH	CMH	ILN
CVG	CVG	ILN
DAL	DAL/DFW	FWX
DAY	DAY	ILN
DCA	ADW/BWI/DCA/IAD	FCX/LWX
DEN	DEN	FTG
DFW	DAL/DFW	FWS
DTW	DTW	DTX
EWR	EWR/JFK	CCX/DIX/OKX
FLL	FLL/MIA/PBI	AMX
HOU	HOU/IAH	HGX
IAD	ADW/BWI/DCA/IAD	FCX/LWX
IAH	HOU/IAH	HGX
ICT	ICT	ICT
IND	IND	IND
JFK	EWR/JFK	CCX/DIX/OKX

TDWR Airport	TDWR(s)	NEXRAD(s)
LAS	LAS	ESX
LGA	EWR/JFK	CCX/DIX/OKX
MCI	MCI	EAX/TWX
MCO	MCO/TPA	MLB/TBW
MDW	MDW/MKE/ORD	LOT/MKX
MEM	MEM	NQA
MIA	FLL/MIA/PBI	AMX
MKE	MDW/MKE/ORD	LOT/MKX
MSP	MSP	MPX
MSY	MSY	LIX
OKC	OKC	CRI
ORD	MDW/MKE/ORD	LOT/MKX
PBI	FLL/MIA/PBI	AMX
PHL	PHL	DIX/DOX
PHX	PHX	IWA
PIT	PIT	PBZ
RDU	RDU	RAX
SDF	SDF	LVX
SJU	SJU	JUA
SLC	SLC	MTX
STL	STL	LSX
TEB	EWR/JFK	CCX/DIX/OKX
TPA	MCO/TPA	MLB/TBW
TUL	TUL	INX

GLOSSARY

ASR-9	Airport Surveillance Radar-9
ARENA	area noted for attention
DoD	Department of Defense
DTED	Digital Terrain Elevation Data
FAA	Federal Aviation Administration
ITWS	Integrated Terminal Weather System
LGA	LaGuardia
LLWAS	Low Level Wind Shear Alert System
MAWA	microburst alert warning area
NEXRAD	Next Generation Weather Radar
PoD	Probability of Detection
RMSE	root-mean-square error
SCR	signal-to-clutter ratio
SLEPs	service life extension programs
TDWR	Terminal Doppler Weather Radar
TEB	Teterboro
TWINDS	Terminal Winds
WSP	Weather Systems Processor

REFERENCES

Airports Council International, 2006: *2005 Annual Worldwide Airport Traffic Report*. Airports Council International, Geneva, Switzerland, http://www.aci.aero/cda/aci/display/main/aci_content.jsp?zn=aci&cp=1-5-54-57_9_2__.

Allan, S. S., and J. E. Evans, 2005: Operational benefits of the Integrated Terminal Weather System (ITWS) at Atlanta. Project Rep. ATC-320, MIT Lincoln Laboratory, Lexington, MA, 149 pp.

Allan, S. S., S. G. Gaddy, J. E. Evans, 2001: Delay causality and reduction at the New York City airports using terminal weather information systems. Project Rep. ATC-291, MIT Lincoln Laboratory, Lexington, MA, 59 pp.

Allan, S., R. DeLaura, B. Martin, D. A. Clark, and C. Gross, 2004: Advanced Terminal Weather Products demonstration in New York. Preprints, *11th Conf. on Aviation, Range, and Aerospace Meteorology*, Hyannis, MA, Amer. Meteor. Soc., http://ams.confex.com/ams/pdfpapers/81294.pdf.

Bieringer P. E., B. Martin, B. Collins, and J. Shaw, 2004: Commercial aviation encounters with severe low altitude turbulence. Preprints, *11th Conference on Aviation, Range, and Aerospace Meteorology*, Hyannis, MA, Amer. Meteor. Soc., http://ams.confex.com/ams/pdfpapers/81278.pdf.

Biron, P. J., and M. A. Isaminger, 1991: High resolution microburst outflow vertical profile data from Huntsville, Alabama, and Denver, Colorado. Project Rep. ATC-163, MIT Lincoln Laboratory, Lexington, MA, 214 pp.

Cho, J. Y. N., G. R. Elkin, and N. G. Parker, 2005: Enhanced radar data acquisition system and signal processing algorithms for the Terminal Doppler Weather Radar. Preprints, *32nd Conf. on Radar Meteorology*, Albuquerque, NM, Amer. Meteor. Soc., http://ams.confex.com/ams/pdfpapers/96018.pdf.

Cole, R. E., and F. W. Wilson, 1994: The Integrated Terminal Weather System Terminal Winds product. *Linc. Lab. J.*, **7**, 475-502.

Cole, R. E., S. M. Green, and M. R. Jardin, 2000: Improving RUC-1 wind estimates by incorporating near-real-time aircraft reports. *Wea. Forecasting*, **15**, 447-460.

Evans, J., and D. Turnbull, 1989: Development of an automated windshear detection system using Doppler weather radar. *Proc. IEEE*, **77**, 1661-1673.

Federal Aviation Administration, 1987: System requirements statement for the Terminal Doppler Weather Radar System. Order No. 1812.9, Dept. of Transportation, 12 pp.

Heiss, W. H., D. L. McGrew, and D. S. Sirmans, 1990: Nexrad: Next generation weather radar (WSR-88D). *Microwave. J.*, **33**, 79-98.

Interagency, 1981: Terminal area weather radar detection and convective prediction development. Interagency agreement *DTFA01-81-Y-10521* between DOT/FAA and DOC/NOAA.

Isaminger, M., T. Beesley, and B. Martin, 2003: An analysis of a wind shear encounter at the John F. Kennedy International Airport (JFK) on 28/29 April 2003. Project Memorandum No. 43PM Wx-0089, MIT Lincoln Laboratory, Lexington, MA, 20 pp.

Istok, M. J., J. T. Ferree, R. E. Saffle, and B. Bumgarner, 2005: NWS use of FAA radar data—Status and operational considerations. Preprints, *32nd Conf. on Radar Meteorology*, Albuquerque, NM, Amer. Meteor. Soc., http://ams.confex.com/ams/pdfpapers/97307.pdf.

Klingle-Wilson, D., and M. F. Donovan, 1991: Characteristics of gust fronts. Preprints, *4th Int. Conf. on Aviation Weather Systems*, Paris, France, Amer. Meteor. Soc., 387-392.

Smalley, D. J., B. J. Bennett, and R. Frankel, 2005: MIGFA: The machine intelligent gust front algorithm for NEXRAD. Preprints, *32nd Conf. on Radar Meteorology*, Albuquerque, NM, Amer. Meteor. Soc., http://ams.confex.com/ams/pdfpapers/96098.pdf.

Weber, M. E., 1999: Wind shear detection using the next generation airport surveillance radar (ASR-11). Project Rep. ATC-266, MIT Lincoln Laboratory, Lexington, MA, 56 pp.

Weber, M. E., and W. R. Moser, 1987: A preliminary assessment of the thunderstorm outflow wind measurement with airport surveillance radars. Project Rep. ATC-140, MIT Lincoln Laboratory, Lexington, MA, 108 pp.

Weber, M. E., and M. L. Stone, 1995: Low altitude wind shear detection using airport surveillance radars. *IEEE Aerosp. Electron. Syst. Mag.*, **10**, 3-9.

Weber, M. E., and S. W. Troxel, 1994: Assessment of the weather detection capability of an airport surveillance radar with solid-state transmitter. Project Rep. ATC-209, MIT Lincoln Laboratory, Lexington, MA, 71 pp.

Zrnić, D. S., 1977: Spectral moment estimates from correlated pulse pairs. *IEEE Trans. Aerosp. Electron. Syst.*, **13**, 344-354.